Microscopic description of nuclei in the middle of the pf-shell by a shell model calculation with G-matrix interaction

### Hitoshi Nakada

Department of Physics, School of Medicine, Juntendo University Hiraga-gakuendai 1-1, Inba-mura, Inba-gun, Chiba 270-16, Japan Takashi Sebe

Department of Applied Physics, College of Engineering, Hosei University

Kajino-cho 3-7-2, Koganei, Tokyo 184, Japan

and

#### Takaharu Otsuka

Department of Physics, Faculty of Science, University of Tokyo
Hongo 7-3-1, Bunkyo-ku, Tokyo 113, Japan

#### Abstract

Energy levels and electromagnetic properties of 24 nuclides with  $N=28\sim30$  are studied in terms of a large-scale shell model calculation, which contains no newly adjusted parameters. The Kuo-Brown G-matrix interaction is shown to reproduce energy levels of 205 low-lying states of all these nuclei. We evaluate effective charges by incorporating the core-polarization effects caused by the coupling to GQR's. We then compute E2 moments and transition probabilities. The M1 moments and transition rates are calculated by quoting the effective g-factors of Towner, which are obtained by taking into account the meson-exchange and the core-polarization mechanisms. By this microscopic calculation most of the E2 properties and the magnetic moments are reproduced. Although there are agreements and disagreements in the M1 transition rates, the general tendency is reproduced. The (e,e') and (p,p') excitation from the ground state to some low-lying  $2^+$  states is also discussed.

### 1 Introduction

The nuclear shell model has been a basic tool to understand the low energy phenomena of nuclei in terms of the nucleonic degrees of freedom. Although the shell model has been successful in the p- and sd-shell regions[1], it is prohibitively difficult to apply the model to most of heavy nuclei, because of the large size of the model space. The effective interaction between valence nucleons should originate in the interaction between free nucleons. There have been many investigations to derive an effective interaction from a microscopic viewpoint of this sort. The restricted model space which enables us to carry out the shell model calculation makes it necessary to renormalize the interaction. The renormalization appears to be successful in comparison to experiment, although the convergence of the renormalization procedure is still being investigated. Nevertheless, it is known that realistic interactions derived from free-nucleon interactions substantially explain the main features of low-lying states of sd-shell nuclei. An example is the interaction obtained in the earlier work of Kuo and Brown[2].

In the pf-shell, shell model calculations have been attempted for many years. In most earlier calculations, the excitation across the gap at Z, N = 28, as well as those at Z, N = 20 or 40, was ignored. Empirical effective interactions were often employed in those works[3, 4, 5]. Horie and Ogawa reported a shell model calculation for N = 29 and 30 nuclei[6, 7], which reproduces yrast levels systematically. A typical example is  $^{56}$ Fe. We, however, cannot reproduce higher states in the framework of Horie and Ogawa's approach. For instance, the excitation energy of the  $2_3^+$  state of  $^{56}$ Fe is overestimated by 0.4MeV, and that of the  $2_4^+$  state by 0.5MeV. This discrepancy is serious in discussing the mixed-symmetry collective states[8], which have been attracting a certain amount of interest[8, 9, 10, 11, 12].

In contrast to the phenomenological interactions, Kuo and Brown applied their Gmatrix method to the pf-shell region, and derived a realistic interaction on the top of the  $^{40}$ Ca core[13]. The Kuo-Brown interaction has been applied to shell model calculations in the full pf-shell, for  $40 < A \le 44$  nuclei[14]. Though qualitative agreement with the exper-

imental data is found in those calculations, there still remain recognizable discrepancies. A few ways of modification of the interaction have been proposed[15, 16, 17]. However, we should take notice that excitations from the sd-shell may be significantly present in the mass region of  $40 < A \le 44$ . It is worthwhile to test the Kuo-Brown interaction in a sufficiently large model space around the middle of the pf-shell, where low-lying states will minimally be affected by other shells.

Oberlechner and Richert carried out a shell model calculation around <sup>56</sup>Ni[18], by using another realistic interaction. They, however, could not succeed in reproducing the experimental energy levels so well, presumably because of the truncation of the model space.

There have been several attempts to take into account the one-particle excitation from the  $0f_{7/2}$  to the  $1p_{3/2}$  orbit[19]. There have been shell model calculations which included the one-particle excitation from the  $0f_{7/2}$  to any of the  $0f_{5/2}$ ,  $1p_{3/2}$  and  $1p_{1/2}$  orbits[20]. However, the situation has not necessarily improved by this extension of the configurations; the discrepancies with  $Ex(2_3^+)$  and  $Ex(2_4^+)$  of <sup>56</sup>Fe, for instance, remain similar to the results in Ref.[7]. This probably happens because the excitation of two nucleons from the  $0f_{7/2}$  to the higher orbits is crucial and can indeed be driven by the deformation and/or the pairing correlation.

In this paper we show the results of the large-scale shell model calculation for  $20 < Z \le 28$ ,  $28 \le N \le 30$  nuclei, including the excitation of up to two particles (four for  $^{56}$ Ni) from the  $0f_{7/2}$  to the other pf-shell orbits, which seems to be of particular importance in this region, as mentioned just above. It turns out that, if a sufficiently large configuration space is chosen, the Kuo-Brown interaction appears to be quite an excellent effective interaction. The model space and the effective hamiltonian are discussed in more detail in Section 2. In Section 3 calculated energy spectra are shown, in comparison with the observed ones. In Sections 4 and 5, the E2 and M1 properties of those nuclei are analyzed in terms of the operators obtained microscopically. Those results will tell us about the reliability of the shell model wavefunctions, and also how well we can understand the nuclear properties from the nucleonic degrees of freedom. The (e, e') form factors concerning the quadrupole

collectivity are discussed on the same footing as the E2 transitions, in Section 6. The DWBA results of (p, p') differential cross sections are briefly surveyed in Section 7. They also supply a justification of the shell model wavefunctions relevant to the low energy quadrupole collective motion. Section 8 is a summary of this article.

## 2 Model space and effective hamiltonian

We first show the configuration space of our shell model calculation. Assuming <sup>40</sup>Ca to be a doubly magic inert core, we consider configurations such as

$$(0f_{7/2})^{n_1-k} (0f_{5/2}1p_{3/2}1p_{1/2})^{n_2+k},$$
 (1)

where  $n_1$  and  $n_2$  are defined so that k=0 should give the lowest configuration in which the excitation across the gap between  $0f_{7/2}$  and the other three orbits is absent. For instance,  $n_1 = 14$  and  $n_2 = 2$  for  $^{56}$ Fe, since this nucleus has 6 protons and 10 neutrons in the pf-shell. For the nuclei handled in this paper,  $n_1 = (Z - 20) + 8$ ,  $n_2 = N - 28$ . The present model space contains all configurations of k = 0, 1 and 2 for each nucleus. We would like to emphasize that such a large configuration space has never been used except for Refs.[8, 15, 21, 22]. The k = 2 configurations evidently play an essential role in the description of the relaxation of the magicity of Z = N = 28 due to the pairing correlation and the deformation.

Concerning the effective hamiltonian, we adopt the Kuo-Brown hamiltonian on top of the  $^{40}$ Ca core[13]. In this hamiltonian, the single-particle energies have been determined from experiment;  $\epsilon_{0f_{7/2}} = 0.0 \text{MeV}$ ,  $\epsilon_{0f_{5/2}} = 6.5 \text{MeV}$ ,  $\epsilon_{1p_{3/2}} = 2.1 \text{MeV}$  and  $\epsilon_{1p_{1/2}} = 3.9 \text{MeV}$ . The two-body interaction is derived from the G-matrix based on the Hamada-Johnston potential, assuming the single-particle wavefunction in the harmonic oscillator approximation. We include the 3p-1h correction, which is evaluated by the perturbation. It is noted that there are only few reports of shell model calculations in the pf-shell using such a microscopic interaction without any phenomenological modification. Around the middle of the pf-shell, both the influence of the sd-shell and that of the sdg-shell are ex-

pected to be minimal. The Kuo-Brown interaction seems to be valid in this region, if the configuration space is sufficiently large. Indeed, the success of the Kuo-Brown interaction in the  $k \leq 2$  configuration space was reported for <sup>48</sup>Sc in Ref.[15]. We already showed the validity also in <sup>56</sup>Fe[8], and the extensive application is carried out in this study.

The isospin is automatically conserved, and in the following we will deal with states with the lowest isospin for each nucleus.

In the numerical calculation, we use an M-scheme shell model code newly developed. The Lanczos method is applied for diagonalizing the shell-model hamiltonian[23]. The present model space is one of the largest one available at present. In the M-scheme, the M=0 space has the largest dimension in even-mass nuclei, while the  $M=\pm\frac{1}{2}$  space in odd-mass nuclei. This dimension is displayed for each nucleus in Table 1, as well as the largest dimension in the JT-scheme.

We add some remarks on the effective interaction: the realistic interaction has long been discussed in the sd-shell. The bare G-matrix is insufficient to reproduce the observed energy spectra, and some renormalization is required. Though the 3p-1h correction improves the energy spectra significantly[2], the convergence of the renormalization procedure has been a serious problem. Despite much effort and a certain progress[24], this problem has not been fully solved yet, and it is beyond the scope of this article. We only comment that the 3p-1h correction gives reasonable spectra and that the low-lying energy spectra resulting from an interaction including the higher-order corrections do not look quite different from those obtained by the 3p-1h correction[25].

In the  $20 \le Z < 28$ ,  $20 \le N < 28$  region, there are many intruder states, which are not described within the shell model for the pf-shell. These intruder states will primarily consist of the excitation from the sd-shell orbits to  $0f_{7/2}$ . Whereas one hole in the sd-shell leads to negative-parity states, two-hole configuration could be low in energy owing to collectivity. The proton-neutron interaction should play a dominant role in introducing this collectivity. The coexistence of the intruder configuration significantly influences the spectrum, and cannot be treated within the renormalization scheme of Kuo-Brown's 3p-1h correction, which is based on the perturbation theory. The modification of the Kuo-Brown

Table 1: The largest dimensions in the shell model calculation with  $k \leq 2$  configurations, both in the M-scheme and the JT-scheme. The fourth and fifth columns indicate the spin-parity and isospin for which the dimension in the JT-scheme is largest.

N	nucl.	M-scheme	J	T	JT-scheme
	$^{49}\mathrm{Sc}$	1,561	$\frac{7}{2}, \frac{9}{2}$	$\frac{7}{2}$	210
	$^{50}\mathrm{Ti}$	5,530	4	3	656
	$^{51}\mathrm{V}$	11,676	$\frac{9}{2}$	$\frac{5}{2}$	1,254
28	$^{52}\mathrm{Cr}$	16,544	5	2	1,615
	$^{53}\mathrm{Mn}$	15,883	$\frac{9}{2}$	$\frac{3}{2}$	1,456
	$^{54}$ Fe	10,620	4	1	891
	$^{55}\mathrm{Co}$	4,717	$\frac{9}{2}$	$\frac{1}{2}$	347
	$^{56}\mathrm{Ni}$	1,353	3	1	103
	$^{50}\mathrm{Sc}$	5,550	4	4	740
	$^{51}{ m Ti}$	20,425	$\frac{9}{2}$	$\frac{7}{2}$	2,423
	$^{52}\mathrm{V}$	46,034	5	3	4,963
29	$^{53}\mathrm{Cr}$	68,355	$\frac{9}{2}$	$\frac{5}{2}$	6,929
	$^{54}{ m Mn}$	70,740	5	2	6,751
	$^{55}\mathrm{Fe}$	50,425	$\frac{9}{2}$	$\frac{3}{2}$	4,611
	$^{56}\mathrm{Co}$	24,844	4	1	2,126
	$^{57}\mathrm{Ni}$	7,890	$\frac{7}{2}$	$\frac{1}{2}$	619
	$^{51}\mathrm{Sc}$	13,411	$\frac{9}{2}$	$\frac{9}{2}$	1,774
	$^{52}\mathrm{Ti}$	52,624	4	4	6,207
	$^{53}\mathrm{V}$	123,519	$\frac{9}{2}$	$\frac{7}{2}$	13,574
30	$^{54}\mathrm{Cr}$	195,334	5	3	20,074
	$^{55}\mathrm{Mn}$	211,833	$\frac{9}{2}$	$\frac{5}{2}$	20,992
	$^{56}$ Fe	162,358	5	2	15,457
	$^{57}\mathrm{Co}$	84,978	$\frac{9}{2}$	$\frac{3}{2}$	8,029
	$^{58}\mathrm{Ni}$	29,792	4	1	2,780

interaction discussed in Refs.[15, 16] yields a better agreement in the  $20 \le Z < 28$ ,  $20 \le N < 28$  region, and this may be connected with the influence of the intruder configuration. The influence of the intruder configuration becomes weaker in  $N \ge 28$  nuclei, due to the suppression of the neutron excitation from the sd-shell to  $0f_{7/2}$  by the Pauli blocking. This will also reduce the proton excitation from the  $^{40}$ Ca core through the proton-neutron correlation. On the other hand, as we approach Z = N = 28, the excitation from  $0f_{7/2}$  to  $(0f_{5/2}1p_{3/2}1p_{1/2})$  will grow. In such cases, the extended configuration space currently considered becomes crucial, as can be seen in the following sections.

In Ref.[13], Kuo and Brown tabulated the interaction for the model space consisting of the four pf-shell orbits and  $0g_{9/2}$ . In this study we omit the contribution containing the  $0g_{9/2}$  orbit, because the influence of  $0g_{9/2}$  is not expected to be significant for the nuclei under consideration. We will return to this problem of the model space in Sections 3.3 and 6.

We shall use a mass-number independent interaction; the harmonic oscillator bases have been employed in calculating the G-matrix, with  $\hbar\omega=10.5 \mathrm{MeV}$  in Ref.[13]. The oscillator length assumed usually as  $b \propto A^{1/6}$  varies by only a few percent among the nuclei under consideration, namely  $A=49\sim58$ . The above value  $\hbar\omega=10.5 \mathrm{MeV}$  adopted in Ref.[13] corresponds to  $A\simeq60$  if we take  $\hbar\omega=41.2A^{-1/3}$ . Thus, the G-matrix calculated in Ref.[13] appears to be appropriate for the mass region considered in this study.

## 3 Energy levels

In this Section we systematically show results of the present calculation for energy levels of  $20 < Z \le 28$ ,  $28 \le N \le 30$  nuclei, in comparison with experimental data. The data are quoted from the compilation in Refs.[26]–[35]. We concentrate on the excitation energies and do not discuss the binding energies.

### 3.1 Ground-state configuration and convergence by truncation

Before going to the energy levels, we shall see the ground-state configurations classified in terms of k in Eq.(1). They are shown in Table 2.

Though one might be interested in the Ca isotopes, they are not suitable for the present study. Probably, in the Ca isotopes, we need to take into account the excitation from the sd-shell.

Within the present calculation, it turns out that the ground state of any nucleus is dominated by the k = 0 configuration, as is expected. The ground state of <sup>56</sup>Ni is outside the  $(0f_{7/2})^{16}$  closed-core by 37%. The k = 0 probabilities are around 60% except for Sc isotopes, while about 70% in Sc isotopes. Thus, the ground state is dominated by the k = 0 configuration in all cases studied. The importance of the k = 2 configuration is obvious in Table 2; The probability of the k = 2 configuration is even larger than that of the k = 1 configuration in many of the nuclei under study.

Table 2 shows that, for N=28, 29 and 30, the k=2 probability goes up as Z increases. This observation gives us information whether the wavefunction is converging under the  $k \leq 2$  truncation. This convergence will be referred to as k-convergence. As Z is larger, the proton Fermi energy should be higher. Therefore the valence proton is more susceptible to be excited from  $0f_{7/2}$  to the upper orbits. This proton excitation will induce the excitation of neutrons from  $0f_{7/2}$  through the proton-neutron correlation. In other words, the energy gap above the  $0f_{7/2}$  orbit becomes less important. Consequently, as we approach Z=28, the k-convergence would become relatively worse. The sd-shell configurations, on the other hand, could have a stronger influence for Z close to 20, since the Pauli blocking suppresses to a lesser extent the proton excitation from the sd-shell to  $0f_{7/2}$ . These problems seem to be much less serious in the region  $Z \sim 24$ .

The k=2 probability is slightly smaller in N=29 and 30 than in N=28 isotones. This happens probably because, in N=29 and 30 isotones, the partial occupancy of the neutron  $(0f_{5/2}1p_{3/2}1p_{1/2})$  orbits suppresses the excitation from  $0f_{7/2}$ . Taking into account the diminishing excitations from the sd-shell, the k-convergence is expected to be quite

Table 2: Ground-state configuration in the shell model calculation in terms of the probabilities (%) of each k configuration.

N	nucl.	state	k=0	k = 1	k = 2
	$^{49}\mathrm{Sc}$	$[\frac{7}{2}]_1^-$	68.2	10.3	21.5
	$^{50}\mathrm{Ti}$	$0_1^+$	61.1	14.9	24.0
	$^{51}{ m V}$	$[\frac{7}{2}]_1^-$	60.5	14.7	24.8
28	$^{52}\mathrm{Cr}$	$0_{1}^{+}$	60.8	12.3	26.9
	$^{53}\mathrm{Mn}$	$[\frac{7}{2}]_1^-$	61.3	10.8	27.9
	$^{54}$ Fe	$0_{1}^{+}$	62.2	7.0	30.8
	$^{55}\mathrm{Co}$	$[\frac{7}{2}]_1^-$	63.0	4.5	32.5
	$^{56}\mathrm{Ni}$	$0_{1}^{+}$	63.4	0.0	36.6
	$^{50}\mathrm{Sc}$	$5_1^+$	68.8	14.6	16.6
	$^{51}\mathrm{Ti}$	$[\frac{3}{2}]_1^-$	60.7	19.2	20.1
	$^{52}\mathrm{V}$	$3_{1}^{+}$	56.6	22.9	20.5
29	$^{53}\mathrm{Cr}$	$[\frac{3}{2}]_1^-$	57.3	20.2	22.5
	$^{54}{ m Mn}$	$3_{1}^{+}$	55.5	21.6	22.9
	$^{55}$ Fe	$[\frac{3}{2}]_1^-$	58.4	15.1	26.5
	$^{56}\mathrm{Co}$	$4_{1}^{+}$	59.4	12.1	28.5
	$^{57}\mathrm{Ni}$	$[\frac{3}{2}]_1^-$	60.9	6.3	32.8
	$^{51}\mathrm{Sc}$	$[\frac{7}{2}]_1^-$	70.2	10.8	19.0
	$^{52}\mathrm{Ti}$	$0_{1}^{+}$	62.7	14.8	22.5
	$^{53}\mathrm{V}$	$[\frac{7}{2}]_1^-$	59.8	19.3	20.8
30	$^{54}\mathrm{Cr}$	$0_{1}^{+}$	56.5	20.6	22.9
	$^{55}\mathrm{Mn}$	$[\frac{5}{2}]_1^-$	53.2	25.1	21.7
	$^{56}$ Fe	$0_{1}^{+}$	55.7	17.7	26.6
	<sup>57</sup> Co	$\left[\frac{7}{2}\right]_1^-$	56.8	15.4	27.9
	$^{58}\mathrm{Ni}$	$0_{1}^{+}$	57.7	9.1	33.1

good for N = 29 and 30 nuclei.

According to the above considerations, we anticipate that, among the nuclei under discussion, the k-convergence will be worst for  $^{56}$ Ni. On the other hand, it is possible to diagonalize the shell model hamiltonian for  $^{56}$ Ni in the space containing all the  $k \leq 4$  configurations, which leads to the M-scheme dimension of 497,805. By this calculation, the ground-state energy of  $^{56}$ Ni is lowered by 3.3MeV, and the k=0 probability reduces to 28%. We shall return to this  $k \leq 4$  calculation in Subsection 3.2.

While there seems to be a slight difference in the k-convergence of the wavefunctions, the energy levels are excellently reproduced, as is discussed in detail in the subsequent subsections. We will discuss the convergence also in Sections 4 and 5.8.

## 3.2 <sup>56</sup>Ni, <sup>49</sup>Sc and <sup>55</sup>Co

In the k=0 configuration space, we have a single state with  $J^P=0^+$  in  $^{56}$ Ni, and one with  $J^P=\frac{7}{2}^-$  in  $^{49}$ Sc and  $^{55}$ Co. These spin-parities of the ground states are unchanged in the present calculation, in agreement with experiments.

The first excited levels become too high in  $^{56}$ Ni and  $^{55}$ Co in the  $k \leq 2$  calculation. In order to describe these states, one probably has to consider a softer  $^{56}$ Ni core than the present one. Higher k configurations will be necessary in order to reproduce those levels.

Wong and Davies carried out a shell model calculation for  $^{56}$ Ni by including the  $k \leq 4$  configuration in part[22]. They reported that the Kuo-Brown interaction successfully reproduces the energy spectrum of  $^{56}$ Ni, although their single particle energies are somewhat different from the present ones. There the  $(0f_{7/2})^{16}$  probability of the ground-state wavefunction was 16%. The small  $(0f_{7/2})^{16}$  probability has brought about several discussions[15, 18]. In the  $k \leq 4$  calculation for  $^{56}$ Ni with the present hamiltonian, the ground state seems to have a similar structure to the result of Wong and Davies, though the k = 0 probability is larger in the present result. In Table 3, the excitation energy of the  $2_1^+$  level obtained by the  $k \leq 4$  calculation, as well as by the  $k \leq 2$  calculation, are shown in comparison with the datum. The  $k \leq 2$  calculation yields too high an excitation

Table 3: Comparison of the  $k \leq 2$  and  $k \leq 4$  calculation with the experimental data taken from Refs.[33], for  $Ex(2_1^+)$  (MeV) and  $B(E2; 2_1^+ \rightarrow 0_1^+)$  values  $(e^2 \text{fm}^4)$  in  $^{56} \text{Ni}$ .

quantity		Cal. $(k \le 2)$ Cal. $(k \le 2)$		Exp.
$Ex(2_1^+)$	[MeV]	5.792	2.724	2.701
$B(\text{E2}; 2_1^+ \to 0_1^+)$	$[e^2 \mathrm{fm}^4]$	80.4	80.6	$74 \pm \frac{36}{28}$

Figure 1:

Experimental and calculated energy levels of  $^{56}$ Ni. The experimental data are taken from Ref.[34]. The calculated energy levels are obtained from the present  $k \leq 4$  shell model calculation.

energy, suggesting that the  $k \leq 2$  model space is too small for this state. On the other hand, the observed energy is reproduced quite well by the  $k \leq 4$  calculation. This agreement encourages us in applying the present G-matrix interaction to the nuclei around  $^{56}$ Ni. The  $k \leq 4$  calculation yields a  $0^+$  level at Ex = 2.30MeV, which is strongly dominated by the k = 4 configuration. An unobserved  $2^+$  level also appears at Ex = 2.96MeV in this calculation. It is interesting to know whether or not these levels exist. The low-lying levels of  $^{56}$ Ni obtained by the present  $k \leq 4$  calculation are summarized in Fig.1, in comparison with the data[33]. We note that the indispensable roles of k = 3 and 4 configurations in  $^{56}$ Ni are due to Z = N = 28 and also due to that neither excited  $0^+$  nor  $2^+$  is allowed with k = 0.

In <sup>49</sup>Sc, no negative-parity states have been observed below Ex = 3MeV other than the ground state. Nevertheless there emerge about ten negative-parity states in 2.4 < Ex < 3MeV in the calculation. Since <sup>49</sup>Sc is far from  $\beta$ -stable line, those states may not have been observed yet. Because  $Z \sim 20$ , the influence of the excitation from the sd-shell

#### Figure 2:

Energy levels of  $^{57}$ Ni. The experimental data are taken from Ref.[34]. The calculated energy levels are obtained from the present  $k \leq 2$  shell model calculation.

may be sizable in comparison with the larger Z case.

## 3.3 $^{57}$ Ni

Suppose that  $^{56}$ Ni is taken to be an inert core, there is only one valence neutron in the  $^{57}$ Ni nucleus. Therefore we have only three states with  $J^P = \frac{1}{2}^-, \frac{3}{2}^-, \frac{5}{2}^-$  in the k = 0 configuration.

In Fig.2, the calculated and measured energy levels are compared. The agreement is sufficiently good for the lowest three states, which predominantly consist of the k=0 configuration. On the other hand, the energy gap between the lowest three states and the other states is larger in the calculation than in the experiment, similarly to  $^{56}$ Ni and  $^{55}$ Co. A larger model space will be necessary for these higher states.

In the k=0 space with the same hamiltonian, we have too low an energy for the  $\left[\frac{5}{2}\right]_1^-$  state (Ex=0.28MeV). The k=1 and 2 configurations improves the energy by raising the  $\left[\frac{5}{2}\right]_1^-$  relative to the  $\left[\frac{3}{2}\right]_1^-$  and  $\left[\frac{1}{2}\right]_1^-$  states.

Note that no  $J^P = \frac{9}{2}^+$  state is observed as low as the  $\left[\frac{3}{2}\right]_1^-$ ,  $\left[\frac{5}{2}\right]_1^-$  and  $\left[\frac{1}{2}\right]_1^-$  levels. A candidate of  $\left[\frac{9}{2}\right]_1^+$  is reported experimentally around Ex = 3 MeV at lowest[34]. This fact suggests that we do not have to include the  $0 \text{g}_{9/2}$  orbit explicitly, as far as we restrict ourselves to the states below about 3 MeV.

Recently phenomenological interactions in the pf-shell, named FPD6 and FPMI3, have been proposed[37]. These interactions are adjusted for the full pf-shell calculation in  $40 < A \le 44$  nuclei and Ca isotopes. It is worthwhile testing these interactions in the

#### Figure 3:

Energy levels of <sup>50</sup>Ti. The data are taken from Ref.[27].

#### Figure 4:

Energy levels of <sup>52</sup>Cr. The data are taken from Ref.[29].

present mass region.

In the  $k \leq 2$  space, neither FPD6 nor FPMI3 reproduces the <sup>57</sup>Ni spectrum; FPD6 makes the  $\left[\frac{5}{2}\right]_1^-$  lower than the  $\left[\frac{3}{2}\right]_1^-$  by 0.5MeV, while in the case of FPMI3, both the  $\left[\frac{5}{2}\right]_1^-$  and the  $\left[\frac{1}{2}\right]_1^-$  become lower than the  $\left[\frac{3}{2}\right]_1^-$  by 2.5 and 1.4MeV, respectively. Note that the probabilities of the k=0 configuration are larger than in the case of the Kuo-Brown interaction for those three lowest-lying states. Thus, those FPD6 and FPMI3 results are less sensitive to higher k configurations. Both FPD6 and FPMI3 are work better for lighter pf-shell nuclei[37].

## **3.4** Z = even, N = 28 nuclei

The energy levels in  $^{50}$ Ti,  $^{52}$ Cr and  $^{54}$ Fe are displayed in Figs.3, 4 and 5. We find that the low-lying states correspond well to the observed levels, in the energy range of  $Ex \lesssim 4 \text{MeV}$ , and with deviations of  $\delta E \lesssim 0.3 \text{MeV}$ .

In  $^{50}$ Ti, the  $4_2^+$  and  $3_1^+$  states appear around 3.5MeV in our calculation, whereas they are not seen in experiments. The occurrence of such additional levels resembles the case

## Figure 5:

Energy levels of  $^{54}$ Fe. The data are taken from Ref.[31].

of  $^{49}$ Sc. The calculated  $0_2^+$  state corresponds well in energy to the unestablished  $0^+$  state. In  $^{54}$ Fe, the number of observed states is larger than that of the calculated ones,

probably due to the model-space restriction. We note that the observed  $0_2^+$  and  $2_2^+$  states, which are missing in the present calculation, might belong to a deformed rotational band, since the energy interval between the two states is much smaller than that between  $0_1^+$  and  $2_1^+$ .

Within the k=0 configuration space, we have only four states with  $J^P=0^+, 2^+, 4^+, 6^+$  in  $^{50}$ Ti and  $^{54}$ Fe. These states consist in the identical energy spectra between  $^{54}$ Fe and  $^{50}$ Ti, as a consequence of the particle-hole symmetry. It is noted here that, within the k=0 configuration,  $Ex(2_1^+)=1.02 \text{MeV}$  is obtained by the present hamiltonian for  $^{50}$ Ti and  $^{54}$ Fe. The experimental energies are 1.55MeV for  $^{50}$ Ti and 1.40MeV for  $^{54}$ Fe, respectively. The present calculation within the  $k\leq 2$  space improves the  $2_1^+$  levels to a great extent, somehow overshooting. Namely, due to the additional pairing correlations associated with the k=1 and 2 configurations, the  $2_1^+$  energies are raised relative to the ground-state energies.

There are two  $4^+$  states around 2.5MeV in  $^{52}$ Cr. This approximate degeneracy is reproduced in the present calculation, where both of the two states predominantly consist of the k=0 configuration. The correspondence of these states between calculation and experiment is tentatively made according to the electromagnetic properties, as will be stated in Sections 4 and 5. The observed  $0_2^+$  and  $2_2^+$  states might be deformed states, as in the case of  $^{54}$ Fe.

#### Figure 6:

Energy levels of <sup>51</sup>V. The data are taken from Ref.[28].

#### Figure 7:

Energy levels of <sup>53</sup>Mn. The data are taken from Ref.[30].

## **3.5** Z = odd, N = 28 nuclei

As shown in Figs.6 and 7, the present calculation reproduces the observed levels in Z = odd, N = 28 nuclei with the energy range of  $Ex \lesssim 3 \text{MeV}$ , which is smaller than in the Z = even case. This is a reasonable consequence, because ground-state energies in even-even nuclei are systematically lower than those in neighboring odd nuclei, owing to the pairing correlation. Indeed, in the present case, this is reflected in the higher level densities in odd nuclei around the ground states.

By comparing Figs.6 and 7, a notable similarity is found for the lowest five levels between  $^{51}$ V and  $^{53}$ Mn, analogously to the similarity between  $^{50}$ Ti and  $^{54}$ Fe. Within the space consisting only of the k=0 configuration, this can be understood as a result of the particle-hole symmetry. The results in Figs.6 and 7 include the k=1 and 2 configurations, which break the simple picture of the particle-hole symmetry. Nevertheless, for the lowest five levels, the properties of this particle-hole symmetry remain to a certain extent in the present calculation. Such properties are seen experimentally also. On the other hand, the similarity disappears in higher states with Ex>2MeV. It is noticed that our calculation

#### Figure 8:

Energy levels of  $^{51}\mathrm{Ti}$ . The data are taken from Ref.[28].

#### Figure 9:

Energy levels of <sup>53</sup>Cr. The data are taken from Ref.[30].

reproduces several levels higher than 2MeV.

## **3.6** Z = even, N = 29 nuclei

The energy levels of  $^{51}$ Ti,  $^{53}$ Cr and  $^{55}$ Fe are shown in Figs.8, 9 and 10, respectively. The good agreement between the calculated and observed ones is confirmed for  $Ex \lesssim 3$ MeV, as in the case of the Z=odd nuclei discussed in Subsection 3.5.

In <sup>51</sup>Ti there is an unobserved  $\frac{7}{2}$  level at 2.9MeV (labeled as  $\left[\frac{7}{2}\right]_2$  in Fig.8) in the present calculation. Concerning this level, we find a similar pattern in the energy spectra

#### Figure 10:

Energy levels of  $^{55}$ Fe. The data are taken from Ref.[32].

#### Figure 11:

Energy levels of <sup>50</sup>Sc. The data are taken from Ref.[27].

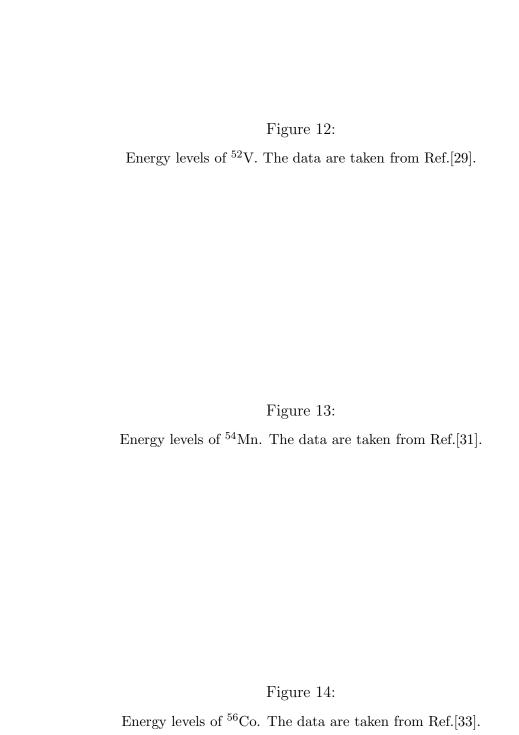
of  ${}^{53}$ Cr and  ${}^{55}$ Fe, in which the  $[\frac{7}{2}]_2^-$  is observed just above the  $[\frac{7}{2}]_1^-$ . When the good agreement around this level and the systematics over these three nuclei are considered, the occurrence of the  $[\frac{7}{2}]_2^-$  state is very likely. It is of interest whether this level is observed in the future experiment or not.

We now compare the present results with those by Horie and Ogawa[6], which have been the most successful shell model calculation in this region. It should be recalled that only the k=0 configuration is included in the Horie-Ogawa calculation. Low-lying levels in N=29 nuclei are fitted in determining the proton-neutron interaction in the Horie-Ogawa calculation. Up to Ex=2MeV, the two results are very similar except for the  $\left[\frac{7}{2}\right]_2^-$  state, in any of  $^{51}$ Ti,  $^{53}$ Cr and  $^{55}$ Fe (See Figs.3–5 of Ref.[6]). The Horie-Ogawa calculation does not produce  $\left[\frac{7}{2}\right]_2^-$  levels in  $^{53}$ Cr and  $^{55}$ Fe, which have been observed close to  $\left[\frac{7}{2}\right]_1^-$  in energy. This is consistent with our observation that the k=1 configuration dominates the  $\left[\frac{7}{2}\right]_2^-$  state of  $^{53}$ Cr and  $^{55}$ Fe. The correspondence between the calculated and experimental  $\frac{7}{2}^-$  levels which are nearly degenerate is made in Fig.9 and 10 on the basis of electromagnetic properties.

## **3.7** Z = odd, N = 29 nuclei

In Figs.11–14, we see a good agreement between the calculated energy levels and experiments for the Z = odd, N = 29 nuclei, as far as the energy range of  $Ex \lesssim 2 \text{MeV}$  is concerned. This smaller energy range of agreement than that for even-even or odd nuclei seems to be associated with the pairing correlation, as has been stated in Subsection 3.5.

Suppose that we restrict the proton and neutron valence orbits only to  $0f_{7/2}$  and  $1p_{3/2}$ 



respectively, only four states are possible in  $^{50}$ Sc;  $J^P=2^+, 3^+, 4^+$  and  $5^+$ . Indeed, the lowest four states consist predominantly of that configuration in the present calculation. The observed 0.257MeV level is expected to have  $J^P=2^+$ . There are several states without the corresponding observed levels in  $^{50}$ Sc. This problem could be accounted similarly as  $^{49}$ Sc is explained.

Among all nuclei that we discuss in this paper, the <sup>52</sup>V nucleus is the only one for which the ground-state spin is not reproduced. This may not be a serious drawback, since the lowest three states are very close in energy and such approximate degeneracy itself is reproduced very well. Based on the present calculation, the observed 0.017MeV state appears most likely to be a 2<sup>+</sup> state. The tentative assignment of 5<sup>+</sup> to the 0.023MeV state seems plausible.

In the Horie-Ogawa results (See Fig.7 of Ref.[6]), the  $4_1^+$  level has energy very close to the lowest three levels  $(5_1^+, 3_1^+ \text{ and } 2_1^+)$ , in contrast to experiment. The present calculation, on the other hand, produces a  $4_1^+$  level nearly degenerate with  $1_1^+$  rather than the lowest three levels, in agreement with the data. The  $5_2^+$  level, which seems to correspond to the observed state at Ex = 0.881 MeV, is dominated by the k = 1 configuration. The occurrence of this level is one of the advantages of the present large-scale calculation, while this k = 1 dominance explains why the Horie-Ogawa interaction is not capable of describing this state.

It is demonstrated that the lowest five states of  $^{54}$ Mn are excellently reproduced. We confirm that the present result is better than the result of the Horie-Ogawa calculation even for these lowest states. There are several k=1 dominant states among the displayed levels; for instance,  $6_1^+$ ,  $1_1^+$ ,  $2_2^+$  and  $7_1^+$ . The low energy of the  $6_1^+$  cannot be described by the Horie-Ogawa k=0 calculation (See Fig.8 of Ref.[6]), which yields  $Ex(6_1^+) \simeq 2$ MeV. Despite a certain underestimation ( $\sim 0.4$ MeV), the reproduction of the low  $Ex(6_1^+)$  is a prominent advantage of the present approach.

In  $^{56}$ Co, the energy of the  $5_1^+$  level shows a certain improvement from the Horie-Ogawa result (See Fig.9 of Ref.[6]). There is an unobserved  $2^+$  state around Ex=1.3MeV in the Horie-Ogawa calculation. Such a state is not seen in the present result. The  $1_1^+$  state

#### Figure 15:

Energy levels of <sup>52</sup>Ti. The data are taken from Ref.[29].

#### Figure 16:

Energy levels of  $^{54}\mathrm{Cr.}$  The data are taken from Ref.[31].

has the k = 1 dominance in the present calculation, consistently with the failure of the description of this state in the Horie-Ogawa calculation.

We cannot reproduce the observed low energy of  $0_1^+$  in  $^{56}$ Co. We should remember, however, that there is no  $0^+$  state in the k=0 configuration. Our calculated  $0_1^+$  level at  $Ex \simeq 2 \text{MeV}$ , whose appearance is encouraging to us, may come down when higher configurations are included.

#### Figure 17:

Energy levels of  $^{56}$ Fe. The data are taken from Ref.[33].

Figure 18:

Energy levels of <sup>58</sup>Ni. The data are taken from Ref.[35].

## **3.8** Z = even, N = 30 nuclei

As is already reported in Ref.[8] and is demonstrated in Fig.17, the spectrum of  $^{56}$ Fe seen in experiments is excellently reproduced for  $Ex \lesssim 4 \text{MeV}$ , apart from the  $3^-$  state of 3.07MeV, which is obviously outside the present configuration space. Discrepancies in the excitation energies are less than 0.2MeV. The calculated excitation energies of the yrast states also agree with the experimental ones up to  $J^P = 8^+$ ; 4.75MeV (4.70MeV in experiment) for  $7_1^+$ , 5.32MeV (5.26MeV) for  $8_1^+$ .

The energy levels of <sup>52</sup>Ti and <sup>54</sup>Cr are displayed in Figs.15 and 16, respectively. There are a few calculated but unobserved levels in <sup>52</sup>Ti. It is not clear, as in the case of <sup>49</sup>Sc, whether those levels emerge because the effect of the sd-shell configuration is too small in the present calculation, or whether they have not been observed.

The comparison with the data of  $^{58}$ Ni is presented in Fig.18. The calculated  $0_2^+$  state is much lower than the experimental one. However, the calculated  $0_2^+$  is highly dominated by the k=2 configuration. It is possible that this remarkable difference of the wavefunction from the ground state makes it difficult to observe the state. If we consider the calculated  $0_3^+$  state to correspond to the observed second  $0^+$ , the agreement becomes satisfactory. We then predict a  $0^+$  state around 2.2MeV. The  $2_3^+$  state is also dominated by the k=2 configuration. The  $B(\text{E2};2_3^+\to 0_2^+)$  value is fairly large  $(200[e^2\text{fm}^4])$  in the present calculation, suggesting a quasi-band structure. Although, in Fig.18, a correspondence of the  $2_3^+$  state to the observed  $2_3^+$  state is tentatively indicated based on their energies, this correspondence can be reconsidered. The calculated  $2_3^+$  state might also remain unobserved. The comparison between calculation and experiment, however, is not

#### Figure 19:

Energy levels of  $^{51}\mathrm{Sc.}$  The data are taken from Ref.[28].

#### Figure 20:

Energy levels of <sup>53</sup>V. The data are taken from Ref.[30].

disturbed by this open question so much.

## **3.9** Z = odd, N = 30 nuclei

The calculated and observed energy levels are exhibited in Figs.19–22, for Z = odd, N = 30 nuclei. There are plenty of low-lying states whose spins and/or parities are not assigned, in these nuclei. We can give a theoretical suggestion.

In  ${}^{51}$ Sc, the spin-parity of the fourth lowest state is  $\frac{9}{2}^-$  in the calculation, while  $\frac{3}{2} \le J \le \frac{7}{2}$  is suggested in the experiment, based on the log ft value of the  $\beta$ -decay from

#### Figure 21:

Energy levels of  $^{55}\mathrm{Mn}$ . The data are taken from Ref.[32].

#### Figure 22:

Energy levels of <sup>57</sup>Co. The data are taken from Ref.[34].

 $^{51}$ Ca[36]. It is desired to specify the spin-parity of this state. According to the present calculation, the observed state with Ex=1.394MeV should have  $J^P=\frac{5}{2}^-$ , which is consistent with the experimental indications. The spin-parity of the 1.715MeV state is considered to be  $\frac{7}{2}^-$ .

In  ${}^{53}\text{V}$ , the calculation strongly suggests the  $J^P = \frac{9}{2}^-$  assignment for the Ex = 1.266MeV state,  $\frac{3}{2}^-$  for the 1.550MeV state and  $\frac{9}{2}^-$  for the 1.653MeV state. None of these suggestions contradict the experiments[30].

In <sup>55</sup>Mn, the data imply an extraordinary situation that three states are present around Ex = 1.29 MeV with surprising degeneracy ( $\Delta E = 0.003 \text{MeV}$ ). Only an  $\frac{11}{2}^-$  state appears in the calculation.

The existence of the  $\frac{3}{2}^-$  state at 1.757MeV in  $^{57}$ Co is not explained within the present model space. This state might be an intruder state dominated by k > 2 configuration.

As a whole, the energy levels of the  $Z=odd,\,N=30$  nuclei are pertinently described by the present calculation, up to  $Ex\simeq 2.5 {\rm MeV}.$ 

## 3.10 Summary of energy levels

We summarize this section. The energy levels of the  $20 < Z \le 28$ ,  $28 \le N \le 30$  nuclei are well reproduced by the present work, where the large-scale shell model calculation in the  $k \le 2$  space is carried out by adopting the Kuo-Brown interaction. The upper bounds of the agreement with the experiments are  $Ex \simeq 4 \text{MeV}$  for even-even, 2.5MeV for odd-mass and 2MeV for odd-odd nuclei. The discrepancy is  $\delta E \lesssim 0.3 \text{MeV}$ .

Most of the low-lying states are, as are expected, dominated by the k=0 configuration.

In odd-odd nuclei, a certain improvement from the Horie-Ogawa result, which contains only the k=0 configuration, is achieved even for the lowest-lying k=0 dominant states. Some low-lying states are found to have larger probabilities of the k=1 configuration than of the k=0 configuration;  $3_1^+$  and  $4_3^+$  of  ${}^{52}\mathrm{Cr}$ ,  $[\frac{13}{2}]_1^-$ ,  $[\frac{11}{2}]_2^-$  and  $[\frac{1}{2}]_1^-$  of  ${}^{53}\mathrm{Mn}$ , one of the nearly degenerate  $\frac{7}{2}^-$  of  ${}^{51}\mathrm{Ti}$ ,  ${}^{53}\mathrm{Cr}$  and  ${}^{55}\mathrm{Fe}$ ,  $5_2^+$ ,  $3_3^+$  and  $4_3^+$  of  ${}^{52}\mathrm{V}$ ,  $6_1^+$ ,  $1_1^+$ ,  $2_2^+$  and  $7_1^+$  of  ${}^{54}\mathrm{Mn}$ ,  $1_1^+$  of  ${}^{56}\mathrm{Co}$ ,  $4_2^+$  and  $2_4^+$  of  ${}^{52}\mathrm{Ti}$ ,  $2_4^+$  and  $3_1^+$  of  ${}^{56}\mathrm{Fe}$ ,  $4_2^+$  of  ${}^{58}\mathrm{Ni}$ ,  $[\frac{3}{2}]_1^-$ ,  $[\frac{1}{2}]_1^-$ ,  $[\frac{7}{2}]_2^-$  and  $[\frac{5}{2}]_1^-$  of  ${}^{57}\mathrm{Co}$ . These levels show good agreement to experiments. We can expect that the wavefunctions of the above k=1 dominant states are as good as those of other low-lying states, since the k=2 probabilities of such states are similar to those of the lowest-lying k=0 dominant states. It is remarked that these k=1 dominant states have been beyond the description by the Horie-Ogawa calculation.

By comparing several effective interactions derived from the G-matrices[13, 18, 38], it is inferred that the G-matrix interaction seems to involve an uncertainty of a few hundred keV. Since this error in the hamiltonian is transferred to the results of the diagonalization, the present discrepancy,  $\delta E \lesssim 0.3 \text{MeV}$ , appears to be quite reasonable. Further investigations will be required in order to discern whether the success of the present calculation is accidental or not. A test of the wavefunctions through the observation of electromagnetic properties is particularly important.

The occurrence of the  $0^+$  level around  $Ex \simeq 2.2 \text{MeV}$  in  $^{58}\text{Ni}$  appears to be a challenging problem. It is strongly desired to search for such a  $0^+$  level experimentally. A search for a  $0^+$  level around  $Ex \simeq 2.3 \text{MeV}$  in  $^{56}\text{Ni}$ , which emerges in the  $k \leq 4$  calculation, is also desired.

## 4 E2 properties

By using the shell model wavefunctions we can investigate the electromagnetic properties of the nuclear states. In this and the next sections we discuss the E2 and M1 properties of the  $N=28\sim30$  nuclei. The purpose of this study is, as well as to test the shell model wavefunctions, to see to what extent we understand the electromagnetic properties of the

nuclei in this region from the nucleonic degrees of freedom without introducing adjustable parameters. We employ single-particle parameter sets of the transitions derived from microscopic theories, which seem to be the most plausible ones presently available. We do not attempt to improve those theories nor to adjust the parameters in this work. The experimental data are taken from Refs.[26]–[35].

### 4.1 Single-particle parameters

The E2 transition (or moment) is described by the following one-body operator of nucleons,

$$T(E2) = \sum_{i} e_i [r_i^2 Y^{(2)}(\hat{\mathbf{r}}_i)],$$
 (2)

where i is the index of nucleons constituting the nucleus. Within the framework of the present shell model, we are dealing only with the valence particles in the pf-shell. Hence the summation in Eq.(2) will be restricted to the nucleons outside the  $^{40}$ Ca core, and the effective charge should be employed in order to incorporate the core polarization effect.

In many cases the effective charges are fitted phenomenologically to experimental data under the assumption of the constancy for many transitions in one or several nuclei. In this paper, however, we derive the effective charges from a microscopic standpoint. In order to take into account the core polarization effect, we use the method of Sagawa-Brown[39], which was shown to work well at least for collective transitions between lowest-lying states in the vicinity of doubly magic core. Then  $e_i$  in Eq.(2) is replaced by  $e_{\rho}^{\text{eff}}(j, j')$ , where  $\rho$  is the subscript for distinguishing between protons and neutrons, and j (j') denotes the initial (final) single-particle orbit of the i-th nucleon.

Although the Kuo-Brown interaction is calculated by assuming the harmonic oscillator single-particle wavefunctions, here we adopt the radial part of the single-particle wavefunctions given by the Hartree-Fock (HF) calculation. Although we abandon the consistency between them, this does not give rise to notable differences as shown later. The HF calculation is carried out with the SGII Skyrme interaction[40] for the  $^{56}$ Ni core, assuming the full occupancy of the  $^{06}$ 7/2 orbit. The isoscalar (IS) and isovector (IV) quadrupole

Figure 23:

Isoscalar and isovector quadrupole response function from the <sup>56</sup>Ni closed core, obtained from the HF+RPA calculation with the SGII Skyrme interaction.

response functions are calculated by the random phase approximation (RPA)[41]. We searched giant quadrupole resonances (GQR) in the range of 10 < Ex < 70 MeV, and find a single isolated IS-GQR peak at  $Ex \simeq 17 \text{MeV}$  and twenty-four IV-GQR peaks distributed over  $Ex = 20 \sim 35 \text{MeV}$ . The response function is defined by

$$S(E) = \sum_{n} |\langle \omega_n^{(\lambda)} | T^{(\lambda)} | 0 \rangle|^2 \delta(E - E_n), \tag{3}$$

where the state  $|0\rangle$  is the HF state,  $|\omega_n^{(\lambda)}\rangle$  an excited RPA state with the angular momentum  $\lambda$ . In this case  $\lambda=2$ , and  $T^{(\lambda)}$  stands for the operator  $r^2Y^{(2)}$  or  $r^2Y^{(2)}\tau_z$ . We show these response functions in Fig.23, taking into account the escaping width. The spreading width is not included in this calculation. By classifying the transition densities at the peak energies through their shapes, we select nine most prominent IV-GQR peaks as well as the IS-GQR peak. The transition strengths are assumed to concentrate in the selected GQR peaks. The adopted peaks and the corresponding transition strengths are listed in Table 4.

The core polarization effect caused by these GQR states is incorporated into the single-particle wavefunctions with the mixing amplitudes evaluated by the perturbation. When a single-particle state is denoted by  $|j\rangle$ , the renormalized single-particle state is written as

$$|\tilde{j}\rangle = |j\rangle + \sum_{n,j'} a_{n,j'}(j) |\omega_n^{(\lambda)} \times j'; j\rangle.$$
 (4)

Table 4:

Excitation energies (MeV) and transition strengths ( $e^2 \text{fm}^4$ ) of the GQR states adopted for the calculation of the core polarization effect. The transition strengths are summed over the states which possess similar shapes of transition densities.

mode	Ex	B(E2)
IS	16.69	800.9
IV	21.83	29.3
	24.64	93.4
	25.60	38.7
	27.19	9.4
	27.69	13.2
	29.77	35.2
	30.21	31.3
	30.93	67.5
	31.86	284.3

Here  $a_{n,j'}(j)$  represents the mixing amplitude evaluated by the perturbation,

$$a_{n,j'}(j) = \frac{\langle \omega_n^{(\lambda)} \times j'; j | V_{\text{res}} | j \rangle}{\epsilon_j - (\epsilon_{j'} + \omega_n^{(\lambda)})}, \tag{5}$$

where  $V_{\text{res}}$  is the residual particle-hole interaction. Then the renormalized transition density is calculated by the perturbation as

$$\langle \tilde{j}' || T^{(\lambda)}(r) || \tilde{j} \rangle \simeq \langle j' || T^{(\lambda)}(r) || j \rangle + \sum_{n} \left\{ a_{n,j'}(j) \langle j' || T^{(\lambda)}(r) || \omega_{n}^{(\lambda)} \times j'; j \rangle + a_{n,j}(j') \langle \omega_{n}^{(\lambda)} \times j; j' || T^{(\lambda)}(r) || j \rangle \right\}$$

$$= \langle j' || T^{(\lambda)}(r) || j \rangle + \sum_{n} \left\{ a_{n,j'}(j) \sqrt{\frac{2j+1}{2\lambda+1}} \langle 0 || T^{(\lambda)}(r) || \omega_{n}^{(\lambda)} \rangle + (-)^{\lambda+j-j'} a_{n,j}(j') \sqrt{\frac{2j'+1}{2\lambda+1}} \langle \omega_{n}^{(\lambda)} || T^{(\lambda)}(r) || 0 \rangle \right\}.$$
 (6)

In the RPA calculation and the evaluation of the mixing amplitudes, the residual interaction  $V_{\text{res}}$  is derived from the SGII Skyrme interaction, consistently with the HF calculation. After taking expectation values of momentum-dependent terms with respect to the HF state, the Skyrme interaction  $H_{Sk}$  only depends on the isoscalar nucleon density  $\rho_{IS}(\mathbf{r})$  and the isovector nucleon density  $\rho_{IV}(\mathbf{r})$ . Therefore the residual interaction is written as

$$V_{\text{res}} = \frac{1}{2} \left. \frac{\delta^2 H_{\text{Sk}}}{\delta \rho_{\text{IS}}^2} \right|_{0} \left[ \sum_{i} \delta(\mathbf{r} - \mathbf{r}_i) \right]^2 + \frac{1}{2} \left. \frac{\delta^2 H_{\text{Sk}}}{\delta \rho_{\text{IV}}^2} \right|_{0} \left[ \sum_{i} \delta(\mathbf{r} - \mathbf{r}_i) \tau_z(i) \right]^2, \tag{7}$$

where  $|_0$  means the evaluation by the HF state. All steps of this renormalization are carried out at the  $^{56}$ Ni core. It should be stressed that this calculation includes no additional adjustable parameters besides those contained in the Skyrme interaction.

The reason why we start from the  $^{56}$ Ni core is that the nuclei under consideration have masses closer to  $^{56}$ Ni than to  $^{40}$ Ca, as a whole. The difference in mass number affects  $\langle r^2 \rangle_{\text{s.p.}}$  (expectation values of  $r^2$  for the single-particle orbits). It is noted that, from the  $^{56}$ Ni core, we have quadrupole transition strength in the  $0\hbar\omega$  space. This  $0\hbar\omega$  strength should be handled principally within the shell model, since we have included the k>0 configuration. The quadrupole transition strength within the  $0\hbar\omega$  space, however, seems to be exhausted in Ex<10MeV, since  $\hbar\omega\sim10\text{MeV}$  at A=56. Indeed we find only a single IS-GQR peak at  $Ex\simeq17\text{MeV}$ , which should be dominated by the  $2\hbar\omega$  configuration. We search the RPA peaks for Ex>10MeV, omitting the strength within the  $0\hbar\omega$  space. By this procedure, the E2 transition strength contributed by the k>2 configurations, which stays within the  $0\hbar\omega$  space but is neglected in the shell model calculation, cannot be included in the following calculation. It should be remembered that the E2 properties, particularly the collective ones, will provide us with a suitable test for the convergence with respect to the  $k\leq2$  truncation.

This renormalization procedure naturally introduces a j-dependence into the effective charges. These j-dependent effective charges are shown in Table 5. It is seen that the j-dependent effective charges are actually insensitive to j. This fact justifies the usual j-independent effective charges for the E2 transition. Recall that the j-independent charges were adopted in Ref.[8], by adjusting the E2 transition probabilities in  $^{56}$ Fe;  $e_{\pi}^{\text{eff}} = 1.4e$  and  $e_{\nu}^{\text{eff}} = 0.9e$ . Comparing the microscopic values in Table 5 with those j-independent effective charges, we have a good agreement for proton charges and a slight suppression for neutron charges. This implies that the core polarization effect is slightly underestimated

Table 5: E2 effective charges evaluated by the method of Sagawa-Brown.

j	j'	$e_{\pi}^{\mathrm{eff}}(j,j')$	$e_{\nu}^{\mathrm{eff}}(j,j')$
$0f_{7/2}$	$0f_{7/2}$	1.354	0.677
$0f_{7/2}$	$0f_{5/2}$	1.482	0.841
$0f_{7/2}$	$1\mathrm{p}_{3/2}$	1.488	0.788
$0f_{5/2}$	$0\mathbf{f}_{5/2}$	1.336	0.643
$0f_{5/2}$	$1p_{3/2}$	1.436	0.712
$0f_{5/2}$	$1p_{1/2}$	1.411	0.690
$1p_{3/2}$	$1\mathrm{p}_{3/2}$	1.341	0.601
$1p_{3/2}$	$1\mathrm{p}_{1/2}$	1.343	0.604

in both IS and IV modes. The influence of the k>2 configurations within the pf-shell might be present in  $^{56}{\rm Fe}$  and this influence may account for the difference in the neutron effective charge. Note that the single-particle matrix elements of  $r^2$  obtained by the HF calculation is very similar to those in the harmonic oscillator approximation, when we use the usual oscillator length  $b=A^{1/6}[{\rm fm}]$  at A=56. In practice, the ratios of the HF matrix elements to the harmonic oscillator ones are  $0.93{\sim}1.05$ . Although there ought to be a certain decrease of the size of the single-particle wavefunctions as A becomes smaller, we will neglect this effect in the following calculation. This decrease amounts only to a 7% reduction of  $B({\rm E2})$  at A=50, by estimating it under the assumption of  $\langle r^2 \rangle_{\rm s.p.} \propto b^2 \propto A^{1/3}$ .

### **4.2** Z = even, N = 28 nuclei

In Table 6, the calculated E2 properties are compared with the measured ones, for Z = even, N = 28 nuclei.

We first see  $B(E2; 2_1^+ \to 0_1^+)$  in these nuclei. In the description only with the k=0 configuration, the identical transition rates are predicted between  $^{50}$ Ti and  $^{54}$ Fe due to the particle-hole conjugation, as far as we neglect the change of the size of the  $0f_{7/2}$  single-particle wavefunction. The present  $k \leq 2$  calculation inherits this feature to a certain extent. Provided that the seniority is conserved as discussed in the work of Horie-Ogawa[6], we also have the same B(E2) value for  $^{52}$ Cr as for  $^{50}$ Ti or  $^{54}$ Fe, within the k=0 space. In the present calculation,  $B(E2; 2_1^+ \to 0_1^+)$  is distinctly enhanced in  $^{52}$ Cr, due to seniority mixing[4] and the influence of the k>0 configurations.

On the other hand, the B(E2) values of  $^{54}{\rm Fe}$  is about twice as large as that of  $^{50}{\rm Ti}$ . The B(E2) value in  $^{52}$ Cr is enhanced from that in  $^{50}$ Ti, while it is close to the value in  $^{54}$ Fe. Although the present calculation is far from reproducing the data for  $^{50}$ Ti and <sup>54</sup>Fe, which has been a problem for a few decades[4], the result in <sup>52</sup>Cr yields a good agreement. As has been discussed in Subsection 3.1, the  $k \leq 2$  truncation might be in sufficient in reproducing some properties of  $^{54}\mathrm{Fe}.$  The k>2 influence may account for the underestimate. In <sup>50</sup>Ti, the sd-shell contribution might be considerable. It is not easy to say whether the stronger mixing of the sd-shell configurations leads to an overestimate or an underestimate, because the adopted effective charges contain the excitation from the sd-shell. The success in <sup>52</sup>Cr, however, may indicate that the amount of core polarization is appropriately evaluated. Since effects of the k>2 configurations are not included in calculating the effective charges, the wavefunctions look almost convergent by the  $k \leq 2$ truncation in this nucleus. It would be impossible to reproduce the rapid change of the B(E2) values without either more precise wavefunctions including the k>2 configurations and the sd-shell excitations explicitly, or a strong particle number dependence of effective charges.

In  $^{52}\mathrm{Cr}$ , there are two  $4^+$  states around 2.5MeV. Judging from  $B(\mathrm{E2};4^+\to2_1^+)$  and

 $B(E2; 6_1^+ \to 4^+)$ , the lower  $4^+$  level in the calculation corresponds rather to the observed  $4_2^+$  state, whereas the higher one to the observed  $4_1^+$  state. This inversion has been taken into account in Fig.4 and Table 6. Through this assignment, we recognize a good agreement between the calculated and measured B(E2) values.

In the k=0 space, the calculated quadrupole moments of the  $2_1^+$  states should have the same magnitudes in  $^{50}$ Ti and  $^{54}$ Fe, while the signs are opposite to each other: positive in  $^{50}$ Ti and negative in  $^{54}$ Fe. Although the signs are maintained, the magnitudes are different in the  $k \leq 2$  calculation. The calculated quadrupole moment in  $^{54}$ Fe is almost twice larger than that in  $^{50}$ Ti. The experimental data contain too large errors to confirm this tendency. In  $^{52}$ Cr,  $Q(2_1^+)$  should be zero under the seniority conservation in the k=0 space. This obviously contradicts with the experiment, which gives a definitely negative value. The present calculation reproduces this property.

The  $B(\text{E2}; 2_1^+ \to 0_1^+)$  value of <sup>56</sup>Ni is already shown in Table 3. The result of the  $k \leq 4$  calculation, as well as that of the  $k \leq 2$  calculation, are compared with the experimental value exhibited in Ref.[33]. Both the  $k \leq 2$  and  $k \leq 4$  calculations give similar values, in good agreement with the datum.

Table 6:

 $B({\rm E2})$  values  $(e^2{\rm fm}^4)$  or E2 static moments  $(e{\rm fm}^2)$  in  $Z=even,\,N=28$  nuclei. The expression i (f) for the second (third) column denotes initial (final) state. The 'Cal.' values are obtained by the present calculation. The experimental data (Exp.) are taken from Refs.[27, 29, 31].

nucl.	i	f	Cal.	Exp.					
$^{50}\mathrm{Ti}$	$2_{1}^{+}$	$0_{1}^{+}$	88.0	$58. \pm 9.$	nucl.	i	f	Cal.	Exp.
	$4_{1}^{+}$	$2_{1}^{+}$	86.8	$60. \pm 13.$	$^{52}\mathrm{Cr}$	61+	$4_1^+$	74.4	$59. \pm 2.$
	$6_{1}^{+}$	$4_1^+$	40.1	$34.4 \pm 1.4$		$6_1^+$	$4_{2}^{+}$	13.2	$29.7 \pm 1.2$
	$0_{2}^{+}$	$2_{1}^{+}$	1.6	$18. \pm 9.$		$4_{3}^{+}$	$4_{2}^{+}$	0.5	$127. \pm 8.$
	$2_{1}^{+}$	$2_{1}^{+}$	9.0*	8. ± 16. *		$3_1^+$	$4_{2}^{+}$	0.2	$7. \pm 5.$
$^{52}\mathrm{Cr}$	$2_{1}^{+}$	$0_{1}^{+}$	102.7	131. $\pm$ 6.		$2_{1}^{+}$	$2_1^+$	$-5.8^*$	$-14. \pm 8. *$
	$4_{1}^{+}$	$2_{1}^{+}$	87.9	$84. \pm 22.$	$^{54}$ Fe	$2_{1}^{+}$	$0_{1}^{+}$	73.3	$128.5 \pm 4.8$
	$4_{2}^{+}$	$2_{1}^{+}$	19.6	$53. \pm 14.$		$4_1^+$	$2_1^+$	68.6	_
	$2_{2}^{+}$	$0_{1}^{+}$	0.05	$0.06 \pm 0.05$		$2_1^+$	$2_1^+$	-16.4*	$-5. \pm 14. *$
	$2_{2}^{+}$	$2_{1}^{+}$	113.4	$150. \pm 35.$		•		•	

<sup>\*)</sup> Quadrupole moment.

# **4.3** Z = odd, N = 28 nuclei

Table 7 shows the E2 quantities in  $Z=odd,\,N=28$  nuclei.

As in the case of  $^{50}$ Ti and  $^{54}$ Fe,  $^{51}$ V and  $^{53}$ Mn are closely related through the particle-hole conjugation within the k=0 space. If the seniority is a good quantum number, any corresponding transitions between low-lying states have the same B(E2) value in these two nuclei, while the quadrupole moments of the corresponding states have identical magnitudes but opposite signs. The present calculation maintains this nature for many E2 transitions. The transition from  $\begin{bmatrix} \frac{5}{2} \end{bmatrix}_1^-$  to  $\begin{bmatrix} \frac{7}{2} \end{bmatrix}_1^-$  is a typical example, which is also confirmed by the experiment. On the other hand, the most significant deviation is seen in  $B(E2; \begin{bmatrix} \frac{3}{2} \end{bmatrix}_1^- \to \begin{bmatrix} \frac{5}{2} \end{bmatrix}_1^-$ ). The B(E2) value of this transition in  $^{51}$ V is almost five times larger than that in  $^{53}$ Mn. These properties are reproduced quite well by the present  $k \leq 2$  calculation.

The results obtained in the present work are remarkably good in  $^{51}$ V. There are certain discrepancies in  $^{53}$ Mn, which cannot be removed without discarding the particle-hole symmetry. This could be an influence of the k>2 configurations.

Table 7:  $B(\text{E2}) \text{ values } (e^2 \text{fm}^4) \text{ or E2 static moments } (e \text{fm}^2) \text{ in } Z = odd, \, N = 28 \text{ nuclei. The}$  experimental data are taken from Refs.[26, 28, 30, 32].

1		c	G 1	Б	nucl.	i	f	Cal.	Exp.
nucl.	i	Ĵ	Cal.	Exp.	$^{53}\mathrm{Mn}$	$[\frac{5}{2}]_1^-$	$[\frac{7}{2}]_1^-$	180.5	$165.\pm\ 35.$
$^{49}\mathrm{Sc}$	$[\frac{7}{2}]_1^-$	$[\frac{7}{2}]_1^-$	$-20.9^*$	_	1,111	_	_		
$^{51}{ m V}$	$[\frac{5}{2}]_1^-$	$[\frac{7}{2}]_1^-$	188.3	$169. \pm 34.$		$[\frac{3}{2}]_1^-$	$[\frac{7}{2}]_1^-$	62.0	$158.\pm\ 13.$
	_	_				$[\frac{3}{2}]_1^-$	$[\frac{5}{2}]_1^-$	22.1	$18.\pm$ 6.
	$[\frac{3}{2}]_1^-$	$[\frac{7}{2}]_1^-$	75.6	89. $\pm$ 10.		$\left[\frac{11}{2}\right]_{1}^{-}$	$[\frac{7}{2}]_1^-$	83.4	$151.\pm\ 21.$
	$[\frac{3}{2}]_1^-$	$[\frac{5}{2}]_1^-$	101.1	$118. \pm 16.$		_		35.4	83.± 11.
	$\left[\frac{11}{2}\right]_{1}^{-}$	$[\frac{7}{2}]_1^-$	95.2	$125. \pm 21.$		$[\frac{9}{2}]_1^-$	$[\frac{7}{2}]_1^-$		
	_		31.6	$37. \pm 6.$		$[\frac{9}{2}]_1^-$	$[\frac{5}{2}]_1^-$	33.9	$44.\pm$ 7.
	$[\frac{9}{2}]_1^-$	$[\frac{7}{2}]_1^-$				$[\frac{1}{2}]_1^-$	$[\frac{5}{2}]_1^-$	0.1	$180.\pm 140.$
	$[\frac{9}{2}]_1^-$	$[\frac{5}{2}]_1^-$	29.9	29. $\pm$ 5.		$\left[\frac{15}{2}\right]_1^-$	$\left[\frac{11}{2}\right]_{1}^{-}$	47.7	$64.\pm 10.$
	$\left[\frac{15}{2}\right]_{1}^{-}$	$\left[\frac{11}{2}\right]_{1}^{-}$	71.6	$66. \pm 8.$		_			04.⊥ 10.
	$\left[\frac{7}{2}\right]_1^-$	$[\frac{7}{2}]_1^-$	$-5.7^{*}$	$-4.3 \pm 0.5^*$		$[\frac{7}{2}]_1^-$	$[\frac{7}{2}]_1^-$	7.5*	
	$\lfloor \frac{1}{2} \rfloor 1$	$\lfloor \overline{2} \rfloor 1$	-0.1	-4.5± 0.5	$^{55}\mathrm{Co}$	$[\frac{7}{2}]_1^-$	$[\frac{7}{2}]_1^-$	20.6*	_

<sup>\*)</sup> Quadrupole moment.

# **4.4** Z = even, N = 29 nuclei

We show the E2 properties of Z = even, N = 29 nuclei in Table 8.

Generally speaking, large errors in experiments make any precise comparison difficult. We only discuss the nearly degenerate  $\frac{7}{2}^-$  states. Let us consider  $B(E2; [\frac{7}{2}]_1^- \to [\frac{3}{2}]_1^-)$  and  $B(E2; [\frac{7}{2}]_2^- \to [\frac{3}{2}]_1^-)$ . The measured  $B(E2; [\frac{7}{2}]_1^- \to [\frac{3}{2}]_1^-)$  value points out the collectivity of this transition. In  $^{53}$ Cr, the calculated transition strength from the higher  $\frac{7}{2}^-$  level agrees with the measured value much better than that from the lower  $\frac{7}{2}^-$  level. We therefore conclude that, in  $^{53}$ Cr, the calculated higher  $\frac{7}{2}^-$  level should correspond to the observed  $[\frac{7}{2}]_1^-$  state, whereas the lower one to the observed  $[\frac{7}{2}]_2^-$  state. This assignment has been taken into account in Fig.9 and Table 8. The transition rates from  $[\frac{11}{2}]_1^-$  and  $[\frac{9}{2}]_1^-$  to these  $[\frac{7}{2}]_1^-$  states support this conclusion. The transition probabilities from the  $[\frac{7}{2}]_1^-$  at the second prefer this reversed correspondence. On the other hand, in  $[\frac{5}{2}]_1^-$  are as we can judge from the transitions to the ground states, the energy sequence of the calculated  $[\frac{7}{2}]_1^-$  and  $[\frac{7}{2}]_2^-$  states seems to be correctly reproduced, as is assigned presently.

Table 8:  $B(\text{E2}) \text{ values } (e^2 \text{fm}^4) \text{ or E2 static moments } (e \text{fm}^2) \text{ in } Z = even, \, N = 29 \text{ nuclei. The}$  experimental data are taken from Refs.[28, 30, 32, 34].

experime	ental dat	ta are ta	aken from F	Refs.[28, 30, 32, 34]	
nucl.	i	f	Cal.	Exp.	
$^{51}{ m Ti}$	$[\frac{1}{2}]_1^-$	$[\frac{3}{2}]_1^-$	102.5		
	$[\frac{7}{2}]_1^-$	$[\frac{3}{2}]_1^-$	82.7	$230. \pm 200.$	
	$[\frac{5}{2}]_1^-$	$[\frac{3}{2}]_1^-$	96.4	$350. \pm 110.$	
	$[\frac{5}{2}]_2^-$	$[\frac{3}{2}]_1^-$	1.0	$49. \pm 10.$	
	$[\frac{5}{2}]_2^-$	$[\frac{1}{2}]_1^-$	80.6	$100. \pm 21.$	
	$[\frac{5}{2}]_2^-$	$[\frac{7}{2}]_1^-$	20.4	$382. \pm 79.$	
	$[\frac{3}{2}]_2^-$	$[\frac{3}{2}]_1^-$	37.5	$376. \pm 12.$	
	$[\frac{11}{2}]_1^-$	$[\frac{7}{2}]_1^-$	110.1	95. $\pm$ 17.	
	$[\frac{15}{2}]_1^-$	$[\frac{11}{2}]_1^-$	59.8	$62. \pm 24.$	
	$[\frac{3}{2}]_1^-$	$[\frac{3}{2}]_1^-$	-11.3*	_	
$^{53}\mathrm{Cr}$	$[\frac{1}{2}]_1^-$	$[\frac{3}{2}]_1^-$	209.0	_	
	$[\frac{5}{2}]_1^-$	$[\frac{3}{2}]_1^-$	44.8	$169. \pm 28.$	
	$[\frac{7}{2}]_1^-$	$[\frac{3}{2}]_1^-$	146.1	$124. \pm 11.$	
	$[\frac{7}{2}]_1^-$	$[\frac{5}{2}]_1^-$	10.3	$76. \pm 19.$	
	$[\frac{7}{2}]_2^-$	$[\frac{3}{2}]_1^-$	0.2	$0.26\pm 0.06$	
	$[\frac{7}{2}]_2^-$	$[\frac{5}{2}]_1^-$	0.0003	$1.9 \pm 1.7$	
	$[\frac{5}{2}]_2^-$	$[\frac{3}{2}]_1^-$	46.9	$43. \pm 19.$	
	$[\frac{5}{2}]_2^-$	$[\frac{7}{2}]_1^-$	27.7	$470. \pm 470.$	
	$[\frac{11}{2}]_1^-$	$[\frac{7}{2}]_1^-$	132.9	$110. \pm 12.$	
	$[\frac{11}{2}]_1^-$	$[\frac{7}{2}]_2^-$	5.2		
nucl.	i	f	Cal.	Exp.	
$^{53}\mathrm{Cr}$	$\left[\frac{11}{2}\right]_2^-$	$[\frac{7}{2}]_1^-$	18.2	_	
	$[\frac{11}{2}]_2^-$	$[\frac{7}{2}]_2^-$	66.1	_	
	$[\frac{9}{2}]_1^-$	$[\frac{7}{2}]_1^-$	0.8	_	
	$[\frac{9}{2}]_1^-$	$[\frac{7}{2}]_2^-$	306.8	270. $\pm 110$ .	
	$[\frac{3}{2}]_2^-$	$[\frac{3}{2}]_1^-$	21.9	130. $\pm 260$ .	
	$[\frac{15}{2}]_1^-$	$[\frac{11}{2}]_1^-$	90.9	$30. \pm 12.$	
	$[\frac{15}{2}]_1^-$	$[\frac{11}{2}]_2^-$	$35^{6.1}$	17. $\pm$ 11.	
	$[\frac{3}{2}]_1^-$	$[\frac{3}{2}]_1^-$	-15.4*	$-15. \pm 5. *$	
FF_	.1.				

## **4.5** Z = odd, N = 29 nuclei

In Table 9, the E2 properties are shown for  $Z=odd,\,N=29$  nuclei.

We can notice the overall agreement between the present calculation and the data, though disagreement in the order of magnitude is seen in  $B(E2; 1_1^+ \rightarrow 2_1^+)$  in  $^{54}Mn$ ,  $B(E2; 3_2^+ \rightarrow 3_1^+)$ ,  $B(E2; 1_1^+ \rightarrow 3_1^+)$  and  $B(E2; 6_1^+ \rightarrow 5_1^+)$  in  $^{56}Co$ . As will be discussed later, the M1 properties of the relevant states are reproduced fairly well. Therefore the shell model wavefunctions of these states are probably adequate. These discrepancies may originate from the influence of the k > 2 configurations, or from the variation of the core polarization effect, which is possible since the initial states of the relevant transitions have rather high energy.

Table 9:  $B(\mathrm{E2})$  values  $(e^2\mathrm{fm}^4)$  or E2 static moments  $(e\mathrm{fm}^2)$  in  $Z=odd,\,N=29$  nuclei. The experimental data are taken from Refs.[27, 29, 31, 33].

nucl.	i	f	Cal.	Exp.	, ,	l .		G 1	-
$^{50}\mathrm{Sc}$	3 <sub>1</sub> <sup>+</sup>	5 <sub>1</sub> <sup>+</sup>	24.0	_	nucl.	i	f	Cal.	Exp.
	$4_1^+$	$5_1^+$	3.5		$^{54}\mathrm{Mn}$	$6_1^+$	$5_1^+$	0.003	< 0.02
						$1_{1}^{+}$	$2_1^+$	2.4	$145. \pm 97.$
F0.	51+	51+	$-25.8^*$			$3_1^+$	$3_1^+$	31.6*	33. ± 3. *
$^{52}\mathrm{V}$	$2_1^+$	$3_1^+$	62.0	$< 9. \times 10^5$	<sup>56</sup> Co	3 <sub>1</sub> <sup>+</sup>	4+	47.1	> 3.6
	$5_1^+$	$3_1^+$	75.5	—		$5_1^+$	$4_1^+$	58.3	$760. \pm {}^{1010.}_{510.}$
	$1_{1}^{+}$	$3_1^+$	96.3	_		i			
	$4_{1}^{+}$	$3_1^+$	31.0			$4_{2}^{+}$	$4_1^+$	18.5	< 70.
	$3_1^+$	3 <sub>1</sub> <sup>+</sup>	$3.8^{*}$			$4_{2}^{+}$	$3_1^+$	40.2	< 52.
$^{54}\mathrm{Mn}$	$2_1^+$	$3_1^+$	6.8			$2_1^+$	$4_1^+$	7.1	$25.5 \pm 8.9$
IVIII	_			_		$2_{1}^{+}$	$3_1^+$	3.5	$9. \pm {}^{18.}_{9.}$
	$4_1^+$	$3_1^+$	83.9	$29.\pm 11.$		$5_{2}^{+}$	$4_1^+$	8.7	$13. \pm \frac{23.}{10.}$
	$5_1^+$	$3_1^+$	58.4	109.±		$3_{2}^{+}$	$4_1^+$	5.2	10.2± 8.9
	$5_1^+$	$4_1^+$	118.2	$280.\pm \begin{array}{cc} 720. \\ 220. \end{array}$		$3_2^+$		3.6	89. ±51.
	$3_{2}^{+}$	$3_1^+$	0.4	< 280.		_	$3_1^+$		
	$3_{2}^{+}$	$2_1^+$	172.6	$194.\pm 97.$		$3_{2}^{+}$	$4_2^+$	52.2	$382. \pm \frac{64}{38}$
	$\begin{vmatrix} 2 \\ 3_2^+ \end{vmatrix}$	$4_1^+$	90.8	$120.\pm {}^{680.}_{90.}$		$1_1^+$	$3_1^+$	0.3	$25. \pm 13.$
	_	_				$7_1^+$	$5_1^+$	0.3	< 32.
	$4_{2}^{+}$	$5_1^+$	35.9	$50.\pm {}^{150.}_{50.}$		$6_1^+$	$5_1^+$	46.6	$0.5\pm \begin{array}{cc} 1.7 \\ 0.5 \end{array}$
	$3_3^+$	$2_1^+$	20.3	$17.\pm \begin{array}{cc} 67. \\ 12. \end{array}$		$4_1^+$	$4_1^+$	22.3*	_
	$3_3^+$	$4_1^+$	31.6	$22.\pm \begin{array}{cc} 39. \\ 17. \end{array}$		-1	_1		
				*) Quadrupo	le mome	nt.			

### **4.6** Z = even, N = 30 nuclei

Table 10 exhibits the B(E2) values and quadrupole moments in Z = even, N = 30 nuclei.

In, a good agreement is obtained. The only problem found in  $^{52}$ Ti and  $^{54}$ Cr is the transition from  $2_3^+$  to  $2_1^+$  in both nuclei. It should be noted that for the  $\gamma$ -transition from  $2_3^+$  to  $2_1^+$  in  $^{54}$ Cr, a different E2/M1 mixing ratio from the previous value has recently been reported[10]. The B(E2) value should be reduced if this new value is adopted.

In  ${}^{56}$ Fe, it is found that the present calculation tends to underestimate the B(E2) values. The k>2 configurations will lead to expected larger collectivity. Keeping this in mind, we can recognize overall agreement also in this nucleus. The  $6_2^+$  state has a large E2 transition probability to  $4_1^+$ , indicating a certain collectivity of the state. This B(E2) value is even larger than  $B(E2; 6_1^+ \to 4_1^+)$ . This feature is properly reproduced in the present calculation. There are certain discrepancies in  $B(E2; 1_1^+ \to 2_1^+)$ ,  $B(E2; 4_2^+ \to 4_1^+)$ ,  $B(E2; 6_1^+ \to 4_2^+)$  and  $B(E2; 6_2^+ \to 6_1^+)$ , whose initial states have rather high energy.

The  $B(E2; 2_1^+ \to 0_1^+)$  is quite underestimated in <sup>58</sup>Ni. It has been known that larger effective charges than those used in systematics are needed in order to adjust  $B(E2; 2_1^+ \to 0_1^+)$  in <sup>58</sup>Ni[5]. Shimizu and Arima described the B(E2) value by taking into account the k = 1 and 2 configurations, based on the pseudo-SU(3) picture[42]. Although the present calculation includes the k = 1 and 2 configurations fully, anomalously larger effective charges are still necessary to reproduce the B(E2) value in <sup>58</sup>Ni, as in the case of <sup>54</sup>Fe.

As mentioned in Section 3, the calculated  $0_3^+$  state of  $^{58}$ Ni corresponds rather well in energy to the second lowest  $0^+$  state observed so far. The B(E2) values to  $2_1^+$  and  $2_2^+$  are consistent with this assignment.

Table 10:  $B({\rm E2}) \mbox{ values } (e^2 \mbox{fm}^4) \mbox{ or E2 static moments } (e \mbox{fm}^2) \mbox{ in } Z=even,\, N=30 \mbox{ nuclei.}$  The experimental data are taken from Refs.[29, 31, 33, 35].

p <u>erimen</u>	tai da	ta ar	e taken from	Refs.[29, 31, 33, 3
nucl.	i	f	Cal.	Exp.
$^{52}\mathrm{Ti}$	$2_1^+$	$0_{1}^{+}$	100.2	$138. \pm \frac{104.}{92.}$
	$2_{2}^{+}$	$0_{1}^{+}$	13.7	$31. \pm \frac{23.}{14.}$
	$2_{3}^{+}$	$2_{1}^{+}$	53.7	> 127.
	$4_1^+$	$2_1^+$	134.0	
	$6_1^+$	$4_1^+$	88.6	$123. \pm 22.$
	$2_1^+$	$2_1^+$	$-7.5^{*}$	
$^{54}\mathrm{Cr}$	$2_1^+$	$0_{1}^{+}$	179.1	$173.6 \pm 3.0$
	$4_1^+$	$2_1^+$	237.6	$303. \pm 97.$
	$2_{2}^{+}$	$0_{1}^{+}$	1.2	$10.9 \pm 4.8$
	$2_{2}^{+}$	$2_{1}^{+}$	71.9	$109. \pm 36.$
	$2_{3}^{+}$	$2_{1}^{+}$	5.6	> 291.
	$6_1^+$	$4_1^+$	196.8	$218. \pm 61.$
	$2_{1}^{+}$	$2_1^+$	$-24.5^*$	$-21.$ $\pm$ 8. *
$^{56}\mathrm{Fe}$	$2_{1}^{+}$	$0_{1}^{+}$	164.8	$213.8 \pm 7.6$
	$4_1^+$	$2_{1}^{+}$	229.6	$305. \pm 64.$
	$2_{2}^{+}$	$0_{1}^{+}$	2.7	$6.4 \pm {7.6 \atop 6.4}$
	$2_{2}^{+}$	$2_{1}^{+}$	4.5	$31. \pm 14.$
	$0_{2}^{+}$	$2_{1}^{+}$	6.7	$31. \pm 15.$
	$2_{3}^{+}$	$0_{1}^{+}$	0.6	$0.97 \pm 0.11$
	$2_{3}^{+}$	$2_{1}^{+}$	13.7	$16.5 \pm 5.1$
	$1_{1}^{+}$	$2_{1}^{+}$	0.0004	$110.7 \pm 8.9$
	$4_{2}^{+}$	$2_{1}^{+}$	0.0008	$1.0 \pm \frac{1.1}{1.0}$
	$2_{4}^{+}$	$0_{1}^{+}$	17.2	$10.2 \pm 5.1$
	$2_{4}^{+}$	$2_{1}^{+}$	18.0	$15. \pm \frac{19}{15}$
	$6_1^+$	$4_1^+$	33.4	$50.9 \pm 5.1$

nucl.	i	f	Cal.		Exp.	
$^{56}\mathrm{Fe}$	$3_{1}^{+}$	$2_{1}^{+}$	13.0	7.6	$\pm$ 6.4	
	$3_{1}^{+}$	$4_1^+$	5.39	10.2	$\pm$ 3.8	
	$3_{1}^{+}$	$2_{2}^{+}$	149.3	430.	$\pm 140.$	
	Ι.	1 .				

# **4.7** Z = odd, N = 30 nuclei

In Table 11, the calculated and measured E2 properties are compared for Z=odd, N=30 nuclei.

The agreement of the calculation with the data is good in <sup>53</sup>V and <sup>55</sup>Mn. Although the data in <sup>57</sup>Co are not necessarily reproduced well, we point out that the orders of magnitude are correct for most transitions.

The  $Q([\frac{3}{2}]_1^-)$  value of <sup>57</sup>Co quoted in Ref.[34] is questionable, since it is not even referred to in the original paper[43].

Table 11:  $B(\text{E2}) \text{ values } (e^2 \text{fm}^4) \text{ or E2 static moments } (e \text{fm}^2) \text{ in } Z = odd, \, N = 30 \text{ nuclei. The}$  experimental data are taken from Refs.[28, 30, 32, 34].  $\boxed{ \text{nucl.} \quad i \quad f \quad \text{Cal.} \quad \text{Exp.} }$ 

nucl.	i	f	Cal.	Exp.
$^{51}\mathrm{Sc}$	$[\frac{3}{2}]_1^-$	$[\frac{7}{2}]_1^-$	50.0	_
	$[\frac{11}{2}]_1^-$	$[\frac{7}{2}]_1^-$	22.7	_
	$[\frac{9}{2}]_1^-$	$[\frac{7}{2}]_1^-$	28.2	_
	$[\frac{5}{2}]_1^-$	$[\frac{7}{2}]_1^-$	3.4	_
	$[\frac{7}{2}]_1^-$	$[\frac{7}{2}]_1^-$	-23.8*	_
$^{53}\mathrm{V}$	$[\frac{5}{2}]_1^-$	$[\frac{7}{2}]_1^-$	253.2	_
	$[\frac{3}{2}]_1^-$	$[\frac{7}{2}]_1^-$	162.2	148.± 12.
	$[\frac{11}{2}]_1^-$	$[\frac{7}{2}]_1^-$	153.3	183.± 28.
	$[\frac{15}{2}]_1^-$	$[\frac{11}{2}]_1^-$	157.7	154.± 35.
	$[\frac{7}{2}]_1^-$	$[\frac{7}{2}]_1^-$	$-10.7^*$	_
$^{55}\mathrm{Mn}$	$[\frac{7}{2}]_1^-$	$[\frac{5}{2}]_1^-$	287.2	335.± 99.
	$[\frac{9}{2}]_1^-$	$[\frac{5}{2}]_1^-$	85.8	109.± 14.
	$[\frac{9}{2}]_1^-$	$[\frac{7}{2}]_1^-$	195.6	$286.\pm\ 37.$
	$[\frac{11}{2}]_1^-$	$[\frac{7}{2}]_1^-$	152.6	175.± 15.
	$[\frac{11}{2}]_1^-$	$[\frac{9}{2}]_1^-$	160.3	< 87.
	$[\frac{1}{2}]_1^-$	$[\frac{5}{2}]_1^-$	36.2	144.± 12.
	$[\frac{3}{2}]_1^-$	$[\frac{5}{2}]_1^-$	19.6	41.± 26.
	$[\frac{13}{2}]_1^-$	$[\frac{9}{2}]_1^-$	148.5	99.± 50.
	$[\frac{13}{2}]_1^-$	$[\frac{11}{2}]_1^-$	89.9	40.± 11.
	$[\frac{15}{2}]_1^-$	$[\frac{11}{2}]_1^-$	164.2	96.± 22.
	$[\frac{15}{2}]_1^-$	$[\frac{13}{2}]_1^-$	52.0	$32.\pm\ 20.$
	$[\frac{5}{2}]_1^-$	$[\frac{5}{2}]_1^-$	33.5*	33.± 1. *
nucl.	i	f	Cal.	Exp.
$^{57}\mathrm{Co}$	$[\frac{9}{2}]_1^-$	$[\tfrac{7}{2}]_1^-$	135.3	$241. \pm 29.$
	$[\frac{3}{2}]_1^-$	$[\tfrac{7}{2}]_1^-$	0.08	$6.0 \pm 1.3$
	$\left[\frac{1}{2}\right]_1^-$	$[\frac{3}{2}]_1^-$	480.8	< 23.
	$\left[\frac{11}{2}\right]_1^-$	$[\tfrac{7}{2}]_1^-$	34.1	$78.2 \pm 7.8$
	$\left[\frac{11}{2}\right]_1^-$	$[\frac{9}{2}]_1^-$	$41^{114.9}$	$370. \pm 100.$
	$\left[\frac{7}{2}\right]_2^-$	$\left[\frac{7}{2}\right]_1^-$	4.9	$0.1 \pm 1.6$
	.73	r () a		

# 5 M1 properties

### 5.1 Single-particle parameters

The M1 properties are usually described by the following one-body operator,

$$T(M1) = \sqrt{\frac{3}{4\pi}} \sum_{i} \hat{\mu}_{i}. \tag{8}$$

For the free nucleon, we have

$$\hat{\mu}_i = \begin{cases} \hat{l}_i + g_{s,\pi}^{\text{free}} \hat{s}_i & (i \in \text{proton}) \\ g_{s,\nu}^{\text{free}} \hat{s}_i & (i \in \text{neutron}) \end{cases} , \tag{9}$$

in units of  $\mu_N$ , where  $l_i$  ( $s_i$ ) denotes the orbital (spin) angular momentum of the *i*-th nucleon, and the  $g_s$ 's are spin g-factors with  $g_{s,\pi}^{\text{free}} = 5.58$ ,  $g_{s,\nu}^{\text{free}} = -3.82$ . It is known, however, that the core polarization and the meson exchange current contribute to the M1 properties. The former appears to be the price for the truncation of the model space in the shell model calculation. Especially the quenching of the spin g-factor is required in most cases. Considering the orbit dependence of the single-particle parameters as in the E2 case, we can parametrize the M1 operator as

$$\hat{\mu}_i = g_{l,\rho}^{\text{eff}}(nl)\hat{l}_i + g_{s,\rho}^{\text{eff}}(nl)\hat{s}_i + g_{p,\rho}^{\text{eff}}(nl, n'l')[Y^{(2)}(\hat{\mathbf{r}}_i)s_i]^{(1)} \ (\rho = \pi, \nu), \tag{10}$$

where the  $g_l$ 's are orbital g-factors. The g-factors are, in principle, dependent on n and l quantum numbers of the single-particle orbit. We adopt the microscopic parameters that Towner calculated with the single-particle wavefunctions in the harmonic oscillator approximation [44].

As in the calculation of energy levels and E2 properties, the mass-number dependence of the single-particle parameters is neglected. In the harmonic oscillator approximation, only the radial part varies with mass number. The matrix elements of the  $\hat{l}$  and  $\hat{s}$  operators, which form the bare M1 operator, do not depend on the radial part. Only a part of the correction coming from the core polarization and meson exchange effects will change with A. Therefore the A-dependence of the M1 single-particle parameters will be weak.

Table 12:

B(M1) values  $(\mu_N^2)$  or M1 static moments  $(\mu_N)$  in Z = even, N = 28 nuclei. The 'Cal.' values are obtained by the present calculation. The experimental data (Exp.) are taken from

Refs.	[27,	29,	31	
-------	------	-----	----	--

nucl.	i	f	Cal.	Exp.
$^{50}\mathrm{Ti}$	$2_1^+$	$2_1^+$	2.388*	$2.4$ $\pm$ $0.8$ *
$^{52}\mathrm{Cr}$	$2_{2}^{+}$	$2_1^+$	0.001	$0.0006 \pm 0.0001$
	$2_{3}^{+}$	$2_1^+$	0.009	$0.082 \pm 0.027$
	$4_{3}^{+}$	$4_1^+$	0.920	_
	$4_{3}^{+}$	$4_{2}^{+}$	0.216	$0.358 \pm 0.072$

nucl.	i	f	Cal.	Exp.
$^{52}\mathrm{Cr}$	3 <sub>1</sub> <sup>+</sup>	$4_{2}^{+}$	0.009	$0.013 \pm 0.005$
	$2_1^+$	$2_1^+$	2.732*	$3.00 \pm 0.50^*$
$^{54}\mathrm{Fe}$	$2_1^+$	$2_1^+$	2.732*	2.4 ±0.3 *
	$6_1^+$	$6_1^+$	8.334*	$8.22 \pm 0.18^*$

<sup>\*)</sup> Magnetic moment.

# **5.2** Z = even, N = 28 nuclei

The calculated M1 properties are shown in Table 12, in comparison with the experimental data, for Z = even, N = 28 nuclei.

All the measured magnetic moments are reproduced very well in  $^{50}$ Ti,  $^{52}$ Cr and  $^{54}$ Fe. In the k=0 configuration, the particle-hole conjugation leads to the same  $\mu(2_1^+)$  between  $^{50}$ Ti and  $^{54}$ Fe. This situation approximately holds both in the experiment and in the  $k\leq 2$  calculation. The contributions of the higher configurations, which have been suggested with respect to the E2 quantities, are not clear in the magnetic moments. The  $\mu(2_1^+)$  value of  $^{54}$ Cr is close to those of  $^{50}$ Ti and  $^{54}$ Fe, as is expected if the seniority conservation is satisfied in the k=0 space. It should be mentioned that a smaller experimental value of  $\mu(2_1^+)=2.00\pm0.32[\mu_N^2]$  has been indicated for  $^{54}$ Fe recently[46].

In  $^{52}$ Cr, the B(M1) values from  $4_3^+$  imply that the  $4_1^+$  and  $4_2^+$  assignment performed in Section 4 is reasonable.

## **5.3** Z = odd, N = 28 nuclei

The M1 quantities in Z = odd, N = 28 nuclei are displayed in Table 13.

All the measured magnetic moments are reproduced remarkably well, highlightening the adequacy of the present description with respect to the proton degrees of freedom. According to the particle-hole symmetry in the k=0 space, the same magnetic moments are expected between  $^{51}$ V and  $^{53}$ Mn, as well as between  $^{49}$ Sc and  $^{55}$ Co. This equality is satisfied approximately.

As in the case of  $^{52}$ Cr, the qualitative trend of the B(M1) values is reproduced in  $^{51}$ V and  $^{53}$ Mn. From a quantitative point of view, we point out that the B(M1) values are generally underestimated in the Z = odd or even, N = 28 nuclei.

Table 13:  $B(\text{M1}) \text{ values } (\mu_{\text{N}}^2) \text{ or M1 static moments } (\mu_{\text{N}}) \text{ in } Z = odd, \, N = 28 \text{ nuclei. The experimental}$   $\frac{\text{data are taken from Refs.}[26,\,28,\,30,\,32].}{\text{data are taken from Refs.}[26,\,28,\,30,\,32].}$ 

nucl.	i	f		Cal.		Exp.		
$^{49}\mathrm{Sc}$	$[\frac{7}{2}]_1^-$	$[\frac{7}{2}]_1^-$		5.152*		_		
$^{51}\mathrm{V}$	$[\frac{5}{2}]_1^-$	$[\frac{7}{2}]_1^-$		0.0003 0.00		$0.0053 \pm 0.0003$		
	$[\frac{3}{2}]_1^-$	$[\frac{5}{2}]_1^-$	(	0.0008	0.	$.00007 \pm \ 0.00002$		
	$[\frac{9}{2}]_1^-$	$[\tfrac{7}{2}]_1^-$	(	0.0005	0.	$0.0006 \pm 0.0002$		
	$[\frac{9}{2}]_1^-$	$\left[\frac{11}{2}\right]_1^-$	(	0.033	0.	$.082 \pm 0.045$		
	$[\frac{7}{2}]_1^-$	$[\frac{7}{2}]_1^-$		5.008*	5.	$.149 \pm 0.000^*$		
	$[\frac{5}{2}]_1^-$	$[\frac{5}{2}]_1^-$		3.457*	3.	.86 ± 0.33 *		
nucl.	i	f	f Ca			Exp.		
$^{53}\mathrm{Mn}$	$[\frac{5}{2}]_1^-$	$[\frac{7}{2}]_1^-$		0.0001		$0.0046 \pm 0.0004$		
	$[\frac{3}{2}]_1^-$	$[\frac{5}{2}]_1^-$		0.0009		$0.041 \pm 0.005$		
	$[\frac{9}{2}]_1^-$	$[\frac{7}{2}]_1^-$		0.00006		$0.0021 \pm 0.0005$		
	$[\frac{13}{2}]_1^-$	$\left[\frac{11}{2}\right]_1^-$		0.0009	)	$0.0026 \pm 0.0003$		
	$\left[\frac{15}{2}\right]_{1}^{-}$	$\left[\frac{13}{2}\right]_1^{-}$		0.024		$0.376 \pm 0.072$		
	$[\frac{7}{2}]_1^-$	$[\frac{7}{2}]_1^-$		4.996*		$5.024 \pm 0.007^*$		
	$[\frac{5}{2}]_1^-$	$\left[\frac{5}{2}\right]_1^-$		3.488*		3.25 ±0.30 *		
$^{55}\mathrm{Co}$	$[\frac{7}{2}]_1^-$	$\left[\frac{7}{2}\right]_{1}^{-}$		4.966*		$4.822 \pm 0.003^*$		

<sup>\*)</sup> Magnetic moment.

## **5.4** Z = even, N = 29 nuclei

Table 14 shows the M1 properties for Z = even, N = 29 nuclei.

We first look at  ${}^{57}$ Ni, which could be a good test of the neutron degrees of freedom. In Table 14, the sign of the experimental magnetic moment of  $[\frac{3}{2}]_1^-$ , which has not been specified[47], is conjectured from the calculated value. The adopted sign is consistent with the Schmidt value. The  $\mu([\frac{3}{2}]_1^-)$  and  $B(M1; [\frac{1}{2}]_1^- \to [\frac{3}{2}]_1^-)$  values are overestimated in the present calculation. Since the neutron orbital angular momentum hardly affects the M1 observables, it is suggested that further quenching of  $g_{s,\nu}$  is required for more precise description. Though within the k=0 configuration the M1 transition from  $[\frac{5}{2}]_1^-$  to  $[\frac{3}{2}]_1^-$  is possible only through the  $[Y^{(2)}s]^{(1)}$ -term, the measured probability is significantly larger than expected from a reasonable  $g_{p,\nu}$  value. Analogously, the present calculation underestimates  $B(M1; [\frac{5}{2}]_1^- \to [\frac{3}{2}]_1^-)$  by several orders of magnitude. In order to remedy this problem, we should include higher configuration into the wavefunctions, or two-body terms into the M1 operator.

It should be noticed that the calculated  $\mu(\lceil \frac{7}{2} \rceil_1^-)$  and  $\mu(\lceil \frac{7}{2} \rceil_2^-)$  of  $^{53}$ Cr have opposite signs to each other. The observed  $\mu(\lceil \frac{7}{2} \rceil_1^-)$  prefers to be positive. This fact is consistent with the present assignment based on the B(E2) values in Section 4, in which the indices of the calculated two  $\frac{7}{2}$  states have been inverted against their energy sequence. The signs of the M1 moments of the lowest two  $\frac{7}{2}$  states are correctly reproduced also in  $^{55}$ Fe, even though the absolute value of  $\mu(\lceil \frac{7}{2} \rceil_2^-)$  is underestimated to a certain extent.

The calculated M1 transition rates agree with the data, at least within the order of magnitude, for  ${}^{51}\text{Ti}$ ,  ${}^{53}\text{Cr}$  and  ${}^{55}\text{Fe}$ . The only exception is  $B(\text{M1}; [\frac{7}{2}]_2^- \to [\frac{5}{2}]_1^-)$  in  ${}^{55}\text{Fe}$ , which is not a serious problem since this B(M1) value is small both theoretically and experimentally.

Table 14:  $B(\text{M1}) \text{ values } (\mu_{\text{N}}^2) \text{ or M1 static moments } (\mu_{\text{N}}) \text{ in } Z = even, \, N = 29 \text{ nuclei. The experimental data are taken from Refs.} [28, 30, 32, 34].$ 

nucl.	i	f	Cal.	Exp.
$^{51}\mathrm{Ti}$	$[\frac{1}{2}]_1^-$	$[\frac{3}{2}]_1^-$	0.825	$0.734 \pm 0.090$
	$\left[\frac{5}{2}\right]_{1}^{-}$	$[\frac{3}{2}]_1^-$	0.049	$0.059 \pm 0.018$
	$[\frac{5}{2}]_2^-$	$[\frac{3}{2}]_1^-$	0.002	$0.016 \pm 0.003$
	$[\frac{5}{2}]_2^-$	$[\frac{7}{2}]_1^-$	0.068	$0.013 \pm 0.003$
	$[\frac{5}{2}]_2^-$	$[\frac{5}{2}]_1^-$	0.146	$0.170 \pm 0.032$
	$[\frac{3}{2}]_2^-$	$[\frac{3}{2}]_1^-$	0.085	$0.127 \pm 0.004$
	$[\frac{3}{2}]_2^-$	$[\frac{1}{2}]_1^-$	0.146	$0.516 \pm 0.016$
	$[\frac{3}{2}]_2^-$	$[\frac{5}{2}]_1^-$	1.739	$3.22 \pm 0.11$
	$[\frac{3}{2}]_1^-$	$[\frac{3}{2}]_1^-$	$-0.989^*$	
$^{53}\mathrm{Cr}$	$[\frac{1}{2}]_1^-$	$[\frac{3}{2}]_1^-$	0.653	
	$[\frac{5}{2}]_1^-$	$[\frac{3}{2}]_1^-$	0.003	$0.093 \pm 0.013$
	$[\frac{7}{2}]_1^-$	$[\frac{5}{2}]_1^-$	0.273	$0.082 \pm 0.016$
	$\left[\frac{7}{2}\right]_2^-$	$[\frac{5}{2}]_1^-$	0.001	$0.0075 \pm 0.0005$
	$\left[\frac{7}{2}\right]_2^-$	$[\frac{7}{2}]_1^-$	0.00006	$0.029 \pm 0.003$
	$\left[\frac{5}{2}\right]_2^-$	$[\frac{3}{2}]_1^-$	0.076	$0.050 \pm 0.016$
	$\left[\frac{5}{2}\right]_2^-$	$[\frac{7}{2}]_1^-$	0.310	$0.269 \pm 0.090$
	$\left[\frac{5}{2}\right]_2^-$	$[\frac{7}{2}]_2^-$	0.00000	_
	$[\frac{9}{2}]_1^-$	$[\frac{7}{2}]_1^-$	0.001	
	$[\frac{9}{2}]_1^-$	$[\frac{7}{2}]_2^-$	0.618	$0.315 \pm 0.045$
nucl.	i	f	Cal.	Exp.
$^{53}\mathrm{Cr}$	$[\frac{3}{2}]_2^-$	$[\frac{3}{2}]_1^-$	0.533	$3.6 \pm 7.2$
	$[\frac{3}{2}]_1^-$	$[\frac{3}{2}]_1^-$	$-0.442^*$	-0.475 ± *
	$[\frac{7}{2}]_1^-$	$\left[\frac{7}{2}\right]_1^-$	$2.435^{*}$	2.8 ±4.9 *
	$[\frac{7}{2}]_2^-$	$\left[\frac{7}{2}\right]_2^-$	-0.719*	_
$^{55}$ Fe	$[\frac{1}{2}]_1^-$	$[\frac{3}{2}]_1^-$	0.844	_
	$[\frac{5}{2}]_1^-$	$[\frac{3}{2}]_1^-$	0.0004	$0.005 \pm 0.002$
	$[\frac{7}{2}]_1^-$	$[\frac{5}{2}]_1^-$	0.123	$0.023 \pm 0.016$
	$[\frac{7}{2}]_2^-$	$[\frac{5}{2}]_1^-$	Q <u>.</u> <del>9</del> 0007	$0.0050 \pm 0.0004$
	$[\frac{9}{2}]_1^-$	$\left[\frac{7}{2}\right]_2^-$	0.317	$0.093 \pm 0.027$
	503	r 7 a		

# 5.5 Z = odd, N = 29 nuclei

Table 15 shows the M1 properties for Z = odd, N = 29 nuclei. We obtain good agreement, except for the extremely large  $\mu(4_1^+)$  and  $\mu(5_1^+)$  of  $^{54}$ Mn which are beyond the ordinary shell model description.

Table 15:  $B(\text{M1}) \text{ values } (\mu_{\text{N}}^2) \text{ or M1 static moments } (\mu_{\text{N}}) \text{ in } Z = odd, \, N = 29 \text{ nuclei. The experimental }$   $\text{data are taken from Refs.} [27, \, 29, \, 31, \, 33].$ 

nucl.	i	f	Cal.	Exp.	nucl.	i	f	Cal.	Exp.
$^{50}\mathrm{Sc}$	3 <sub>1</sub> <sup>+</sup>	$2_1^+$	2.099		$^{54}\mathrm{Mn}$	1+	$2_1^+$	0.030	$0.025 \pm 0.014$
30					10111	_			
	$4_1^+$	$5_1^+$	1.748	_		$3_1^+$	$3_1^+$	2.987*	$3.282 \pm 0.001^*$
	$5_1^+$	$5_1^+$	3.980*	_		$4_1^+$	$4_1^+$	3.749*	$7.3~\pm~1.4~^*$
$^{52}\mathrm{V}$	$2_1^+$	$3_1^+$	1.528	$1.33 \pm 0.50$		$5_1^+$	$5_1^+$	4.282*	55. ±30. *
	$1_{1}^{+}$	$2_{1}^{+}$	0.226			$3_{2}^{+}$	$3_{2}^{+}$	4.226*	< 18
	$4_1^+$	$3_1^+$	0.110		$^{56}\mathrm{Co}$	3 <sub>1</sub> <sup>+</sup>	$4_1^+$	2.190	> 0.10
	$4_1^+$	$5_1^+$	0.572			$5_1^+$	$4_1^+$	0.552	$0.72~\pm~0.18$
	$3_{1}^{+}$	$3_1^+$	3.049*			$4_{2}^{+}$	$4_1^+$	0.003	< 0.010
$^{54}{ m Mn}$	$2_{1}^{+}$	$3_{1}^{+}$	1.158			$4_{2}^{+}$	$3_1^+$	0.035	< 0.057
	$4_1^+$	$3_1^+$	0.100	$0.055 \pm 0.005$		$4_{2}^{+}$	$5_1^+$	0.003	< 0.021
	$5_1^+$	$4_1^+$	0.538	$0.591 \pm 0.072$		$2_1^+$	$3_1^+$	0.855	$0.97~\pm~0.27$
	$3_{2}^{+}$	$3_1^+$	0.099	$0.116 \pm 0.025$		$5_{2}^{+}$	$4_1^+$	0.223	$0.088 \pm 0.036$
	$3_{2}^{+}$	$2_{1}^{+}$	0.034	$0.052 \pm 0.013$		$3_{2}^{+}$	$4_1^+$	0.103	$0.125 \pm 0.072$
	$3_{2}^{+}$	$4_1^+$	1.182	$1.00 \pm 0.22$		$3_{2}^{+}$	$3_1^+$	0.006	$0.006 \pm \ 0.003$
	$4_{2}^{+}$	$5_1^+$	0.499	$0.322 \pm 0.072$		$3_{2}^{+}$	$4_{2}^{+}$	0.727	$1.07~\pm~0.54$
	$3_{3}^{+}$	$2_1^+$	0.420	$0.59 \pm 0.14$		$1_{1}^{+}$	$2_{1}^{+}$	0.00006	$0.143 \pm 0.072$
	$3_{3}^{+}$	$4_1^+$	0.245	$0.63 \pm 0.14$		$6_1^+$	$5_1^+$	0.142	$0.125 \pm 0.072$
	$6_1^+$	$5_1^+$	0.0004	$0.0005 \pm 0.0002$		$4_1^+$	$4_1^+$	3.654*	$3.830 \pm 0.015^*$

<sup>\*)</sup> Magnetic moment.

## **5.6** Z = even, N = 30 nuclei

The calculated M1 quantities are compared with the measured ones in Table 16, for Z = even, N = 30 nuclei.

Although the agreement of the B(M1) values is not necessarily good in  $^{56}$ Fe, the orders of magnitudes are correctly reproduced for most transitions. As will be discussed below, the further quenching of  $g_{s,\rho}$  improves the results considerably. The observed  $B(M1; 1_1^+ \to 0_1^+)$  value is quite small. This nature is reproduced well in the present calculation. The discrepancy in  $B(M1; 2_3^+ \to 2_1^+)$  is not improved by the  $g_s$  quenching. The cancellation among the elements of the density matrix brings this small B(M1) value. As discussed in Ref.[8], the  $2_3^+$  state is a fully non-collective state. We should note that non-collective transitions are generally sensitive to details of wavefunctions. The (p, p') result[12] confirms the adequacy of the present shell model wavefunction of this state, as will be mentioned in Section 7.

In Ref.[8], the n and l dependences in Eq.(10) were neglected, as is often assumed. Furthermore,  $g_{p,\rho}^{\text{eff}} = 0$  was assumed. Namely, the employed M1 operator was

$$T(M1) = \sqrt{\frac{3}{4\pi}} \sum_{\rho=\pi,\nu} (g_{l,\rho}^{\text{eff}} \hat{L}_{\rho} + g_{s,\rho}^{\text{eff}} \hat{S}_{\rho}), \tag{11}$$

where

$$\hat{L}_{\rho} = \sum_{i \in \rho} \hat{l}_i, \ \hat{S}_{\rho} = \sum_{i \in \rho} \hat{s}_i. \tag{12}$$

The single-particle g-factors of  $g_{l,\pi}^{\text{eff}} = 1.0$ ,  $g_{l,\nu}^{\text{eff}} = 0.0$ ,  $g_{s,\pi}^{\text{eff}} = 0.5 g_{s,\pi}^{\text{free}}$  and  $g_{s,\nu}^{\text{eff}} = 0.5 g_{s,\nu}^{\text{free}}$  were adopted in Ref.[8] so as to fit the data in  $^{56}$ Fe, though microscopic calculations predict the quenching factor for  $g_{s,\rho}$  to be much closer to the unity[44, 45]. It was shown in Ref.[8] that by this phenomenological set of parameters the B(M1) valued in  $^{56}$ Fe are reproduced reasonably well.

It is found that the predicted  $1_3^+$  state of  ${}^{56}$ Fe, as well as the  $1_2^+$  state, has a relatively large  $B(\mathrm{M1})$  value to the ground state. This fact suggests that these two states contain a considerable fraction of a mixed-symmetry  $1^+$  component. A recent experiment has also reported a mixed-symmetry  $1^+$  strength around  $Ex \simeq 3.5 \mathrm{MeV}[48]$ . We will discuss this

Table 16:  $B(\text{M1}) \text{ values } (\mu_{\text{N}}^2) \text{ or M1 static moments } (\mu_{\text{N}}) \text{ in } Z = even, \, N = 30 \text{ nuclei. The experimental data are taken from Refs.} [29, 31, 33, 35].$ 

,					nucl.	i	f	Cal.	Exp.
nucl.	i	f	Cal.	Exp. 0.41	$^{56}$ Fe	$1_{2}^{+}$	$0_{1}^{+}$	0.061	$0.047 \pm 0.013$
$^{52}\mathrm{Ti}$	$2_{2}^{+}$	$2_1^+$	0.456	$0.56 \pm {0.41 \atop 0.25}$		$1_{2}^{+}$	$2_1^+$	0.048	$0.054 \pm 0.014$
	$2_3^+$	$2_1^+$	0.610	> 0.16		$1_3^+$	$0_1^+$	0.151	
	$2_1^+$	$2_1^+$	0.666*			$1_3^+$	$2_1^+$	0.155	
$^{54}\mathrm{Cr}$	$2_{2}^{+}$	$2_1^+$	0.021	$0.023 \pm\ 0.009$		$2_{5}^{+}$	$2^{+}_{1}$	0.012	$0.003 \pm 0.002$
	$2_{3}^{+}$	$2_1^+$	0.519	> 0.10			_		
	$2_1^+$	$2_1^+$	1.467*	$1.12 \pm 0.20^*$		$6_{2}^{+}$	$6_1^+$	0.274	$1.09 \pm 0.18$
$^{56}\mathrm{Fe}$	$2_{2}^{+}$	2+	0.476	$0.233 \pm 0.072$	<b>T</b> 0	21+	$2_1^+$	1.379*	$1.20 \pm 0.20^*$
	$2_{3}^{+}$	$2_1^+$	0.0005	$0.070 \pm 0.009$	<sup>58</sup> Ni	$2_{2}^{+}$	$2_1^+$	0.156	$0.018 \pm 0.009$
	$1_1^+$	$0_1^+$	0.0004	< 0.00001		$1_1^+$	$0_1^+$	0.00004	$0.0014 \pm 0.0003$
	$1_1^+$	$2_{1}^{+}$	0.090	$0.040 \pm 0.003$		$0_{2}^{+}$	$1_1^+$	0.0001	_
	_	-				$0_{3}^{+}$	$1_{1}^{+}$	0.0005	$0.158 \pm 0.009$
	$4_{2}^{+}$	$4_1^+$	0.841	$0.206 \pm 0.038$		$2_{3}^{+}$	$2_1^+$	0.018	$0.134 \pm 0.021$
	$2_4^+$	$2_1^+$	0.202	$0.109 \pm 0.045$		$2_{3}^{+}$	$2_{2}^{+}$	0.140	$0.555 \pm 0.090$
	31+	$2_1^+$	0.028	$0.054 \pm 0.013$		$2_{4}^{+}$	$2_1^+$	0.030	$0.070 \pm 0.029$
	$3_1^+$	$4_1^+$	0.030	$0.098 \pm 0.023$		3 <sub>1</sub> <sup>+</sup>	$4_1^+$	0.308	$0.16 \pm 0.14$
	$3_1^+$	$2_{2}^{+}$	0.026	$0.018 \pm 0.007$		$2_1^+$	$2_1^+$	-0.168*	_

<sup>\*)</sup> Magnetic moment.

point in more detail in a forthcoming paper. These two states are almost degenerate in energy ( $Ex \simeq 3.5 \text{MeV}$ ) according to the calculation, while only a single state has been experimentally confirmed[33]. It is desired to search for the other state.

We do not have a good agreement for  $^{58}$ Ni. This disagreement might imply a non-negligible influence of the k>2 configurations.

# **5.7** Z = odd, N = 30 nuclei

The M1 properties are shown in Table 17, for  $Z=odd,\,N=30$  nuclei.

The M1 quantities in  $^{55}$ Mn are reproduced remarkably well. Together with the agreement in the E2 properties, this fact suggests good convergence of the wavefunctions in this nucleus. The agreement in  $^{57}$ Co is only for the orders of magnitude.

Table 17:  $B({\rm M1}) \ {\rm values} \ (\mu_{\rm N}^2) \ {\rm or} \ {\rm M1} \ {\rm static} \ {\rm moments} \ (\mu_{\rm N}) \ {\rm in} \ Z = odd, \ N = 30 \ {\rm nuclei}. \ {\rm The \ experimental}$ 

data are taken from Refs.[28, 30, 32, 34].								
nucl.	i	f	Cal.	Exp.				
$^{51}\mathrm{Sc}$	$[\frac{7}{2}]_1^-$	$[\frac{7}{2}]_1^-$	5.061*	_				
$^{53}\mathrm{V}$	$[\frac{5}{2}]_1^-$	$[\frac{7}{2}]_1^-$	0.065	> 0.027				
	$[\frac{3}{2}]_1^-$	$\left[\frac{5}{2}\right]_1^-$	0.00001	$0.0032 \pm 0.0003$				
	$[\frac{7}{2}]_1^-$	$[\frac{7}{2}]_1^-$	4.670*	_				
$^{55}\mathrm{Mn}$	$[\frac{7}{2}]_1^-$	$[\frac{5}{2}]_1^-$	0.042	$0.076 \pm 0.003$				
	$[\frac{9}{2}]_1^-$	$[\frac{7}{2}]_1^-$	0.085	$0.197 \pm 0.021$				
	$[\frac{11}{2}]_1^-$	$[\frac{9}{2}]_1^-$	0.227	$0.224 \pm 0.023$				
	$[\frac{3}{2}]_1^-$	$[\frac{5}{2}]_1^-$	0.147	$0.167 \pm 0.036$				
	$[\frac{13}{2}]_1^-$	$[\frac{11}{2}]_1^-$	0.154	$0.233 \pm 0.054$				
	$[\frac{15}{2}]_1^-$	$\left[\frac{13}{2}\right]_1^-$	0.257	$0.251 \pm 0.072$				
	$[\frac{5}{2}]_1^-$	$[\frac{5}{2}]_1^-$	3.378*	$3.453 \pm 0.001^*$				
	$[\frac{7}{2}]_1^-$	$[\frac{7}{2}]_1^-$	4.477*	$4.4$ $\pm$ $0.7$ *				
57Co	$[\frac{9}{2}]_1^-$	$[\frac{7}{2}]_1^-$	0.304	$0.372 \pm 0.036$				
	$[\frac{1}{2}]_1^-$	$[\frac{3}{2}]_1^-$	0.652	$0.090 \pm 0.011$				
	$[\frac{11}{2}]_1^-$	$[\frac{9}{2}]_1^-$	0.722	$0.877 \pm 0.090$				
nucl	.   i	f	Cal.	Exp.				
<sup>57</sup> Cc	$[\frac{7}{2}]_2^-$	$[\frac{7}{2}]_1^-$	0.002	0.022±0.003				

nucl.	i	f	Cal.	Exp.
$^{57}\mathrm{Co}$	$[\frac{7}{2}]_2^-$	$[\frac{7}{2}]_1^-$	0.002	$0.022 \pm 0.003$
	$[\frac{7}{2}]_2^-$	$[\frac{9}{2}]_1^-$	0.115	$0.662 \pm 0.090$
	$[\frac{5}{2}]_1^-$	$[\frac{7}{2}]_1^-$	0.044	$0.236 \pm 0.032$
	$[\frac{5}{2}]_2^-$	$[\frac{7}{2}]_1^-$	0.002	
	$[\frac{7}{2}]_3^-$	$[\frac{7}{2}]_1^-$	0.032	$0.003 \pm 0.001$
	$[\frac{7}{2}]_3^-$	$[\frac{9}{2}]_1^-$	0.775	$0.100 \pm 0.020$
	$[\frac{9}{2}]_2^-$	$[\frac{7}{2}]_1^-$	0.020	< 0.034
	$[\frac{9}{2}]_2^-$	$[\frac{9}{2}]_1^-$	0.028	< 0.054
	$[\frac{9}{2}]_2^-$	$[\frac{11}{2}]_1^-$	0.001	< 0.21
	$[\frac{9}{2}]_2^-$	$[\frac{7}{2}]_{2}^{-}$	0.004	$0.36 \pm 0.13$
	$[\frac{13}{2}]_1^-$	$[\frac{11}{2}]_1^-$	0.718	$0.73 \pm 0.18$
	$[\frac{15}{2}]_1^-$	$[\frac{13}{2}]_1^-$	<b>3</b> 9.730	$0.233 \pm 0.090$
	$[\frac{7}{2}]_1^-$	$[\frac{7}{2}]_1^-$	4.729*	$4.727\pm0.009^*$
	- 2 -	- 9 -		

## 5.8 Summary of electromagnetic properties

We summarize the consequences for the electromagnetic properties. The E2 transition probabilities and moments are comprehensively reproduced, together with the effective charges derived by the Sagawa-Brown method. The good agreement with the measurement in the collective (i.e., enhanced) E2 transitions suggests that the convergence of the wavefunctions is reasonable in the framework of the  $k \leq 2$  truncation. We also acquire an overall reproduction of the M1 transition rates and moments, by using Towner's single-particle g-factors. Particularly, most of the measured magnetic moments are precisely reproduced. The remaining discrepancies may be ascribed to the k > 2 configuration or the sd-shell contribution.

# 6 Electron scattering form factors

We calculate longitudinal form factors of inelastic electron scattering with an angular momentum transfer of two units (C2), from the ground state to several  $2^+$  states for a few even-even nuclei. The form factors provide us with richer information than the  $\gamma$ -transition probabilities, owing to the off-shell photon exchange. We here attempt to see how well the present calculation reproduces the quadrupole collective feature. The method of Sagawa-Brown[39], which has already been sketched in Section 4, is used again. This method was shown to work very well for longitudinal form factors with collectivity for nuclei around the doubly magic core.

The C2 form factors are calculated from the shell model density matrices, together with the renormalized single-particle transition densities of Eq.(6). The nucleon finite-size effect is incorporated in the dipole approximation[49], and the contribution of the center-of-mass motion is subtracted in the harmonic oscillator approximation[50]. The plane-wave Born approximation (PWBA) is employed, taking into account the Coulomb distortion effect in terms of the effective momentum transfer  $q_{\text{eff}}$ . It should be emphasized that this calculation includes no additional adjustable parameters, as pointed out in Section 4.

The results for <sup>56</sup>Fe were already shown in Ref.[8]. Here we mention that the results

### Figure 24:

(e, e') form factors from the ground state to the lowest four  $2^+$  states of  $^{54}$ Cr. The solid lines show the shell model results with the core polarization effect evaluated by the HF+RPA. Those without core polarization are shown by dotted lines. The crosses exhibit the experimental data taken from Ref.[52]. The transverse mode is not separated in the experiment.

of this calculation agree with the data[51] very well. Particularly, the form factor in the excitation to  $2_1^+$  is in a precise agreement. It is also remarkable that the collectivity of the  $2_4^+$  is correctly reproduced.

The C2 form factors in  $^{54}$ Cr are shown in Fig.24. In the experiments the transverse mode was not separated, though most of the reaction is known to be dominated by the C2 mode[53]. The experimental data are described precisely with respect to the  $2_1^+$  state. As for the  $2_2^+$  state, the shape is reproduced well, though the absolute value is overall underestimated by a factor of 2. It is pointed out that this transition is not collective. There are no reported data with respect to the  $2_3^+$  and  $2_4^+$  states. We show them, however, since they are good candidates for the mixed-symmetry state[11].

The form factors from  $0_1^+$  to  $2_1^+$  in  ${}^{54}$ Fe and  ${}^{58}$ Ni are shown in Fig.25 and Fig.26, respectively. The absolute value is underestimated, and this is consistent with the B(E2) values discussed in Section 4. This might indicate a worse convergence of the wavefunctions for these nuclei. Nevertheless, the shape of the form factors, especially the position of the peaks and the dips are reproduced very well.

### Figure 25:

(e, e') form factor from the ground state to the  $2_1^+$  state of  $^{54}$ Fe. See the caption of Fig.24. The experimental data are taken from Ref.[54].

#### Figure 26:

(e, e') form factor from the ground state to the  $2_1^+$  state of  $^{58}$ Ni. See the caption of Fig.24. The experimental data are taken from Ref.[55].

# 7 Proton scattering cross sections

Recently  $(\vec{p}, p')$  experiments are performed for <sup>56</sup>Fe and <sup>54</sup>Cr[12], with an incident proton energy of 65MeV. The differential cross sections and the analyzing powers are extracted. The data are analyzed in the distorted-wave Born approximation (DWBA), by using the present shell model density matrices. This DWBA calculation is carried out by Takamatsu and his collaborators[12]. We briefly review their results in this section.

The Bonn-Jülich effective interaction [56] is employed as the interaction between the incident or scattered proton and the nucleons in the target nucleus. Although the M3Y interaction [57] and the Paris-Hamburg interaction [58] are tried also, the results were essentially the same. In order to reproduce the experimental data, an overall normalization factor is used for each transition. This factor would correspond to the core polarization effect. In fact, the adjusted normalization factors are consistent with the ones expected from the effective charges employed in the description of the B(E2) values.

The absolute value of the cross section in the excitation to the  $2_3^+$  state is smaller by an order of magnitude than to the  $2_2^+$  or the  $2_4^+$  states in the experimental data of  $^{56}$ Fe. This is consistent with the present calculation. In addition, the excitation to the  $2_3^+$  state shows a strikingly anomalous angular distribution. The present shell model wavefunctions reproduce this anomaly remarkably well.

The experimental differential cross sections are also excellently reproduced for  $^{54}$ Cr[12]. We have not seen any notable contradiction between experiments and the present calculation with respect to (e, e') and (p, p') data.

# 8 Summary

The properties of the low-lying states in  $20 < Z \le 28$ ,  $28 \le N \le 30$  nuclei have been investigated from a microscopic standpoint. The model space has been restricted to the pf-shell, while we have incorporated the excitation from  $0f_{7/2}$  to  $(0f_{5/2}1p_{3/2}1p_{1/2})$  up to two particles. This space leads to one of the largest-scale shell model calculations that have ever been carried out.

We have adopted the Kuo-Brown interaction on top of the  $^{40}$ Ca core, including the 3p-1h correction. This effective interaction is derived from the Hamada-Johnston NN potential, through the G-matrix calculation. Despite the failure near the beginning of the pf-shell, it has been shown for the first time, by this work, that this microscopic interaction produces an excellent description of the nuclei around the middle of the pf-shell.

The observed energy levels are reproduced by the present shell model calculation in a wide range of energy, for any of the  $20 < Z \le 28$ ,  $28 \le N \le 30$  nuclei. The energy range of good agreement is typically  $Ex \le 4 \text{MeV}$  for even-even nuclei,  $Ex \le 2.5 \text{MeV}$  for odd-mass nuclei and  $Ex \le 2 \text{MeV}$  for odd-odd nuclei, with the discrepancies of  $\delta E \le 0.3 \text{MeV}$ . These energy ranges are notably wider than those obtained in previous shell model studies[6, 7, 19, 20], covering the region where candidates for the mixed-symmetry states were reported. Among a number of states dominated by the k = 0 configuration, more than twenty states in the low energy region are found to have k = 1 probabilities

larger than k = 0 ones. The k = 1 dominance of those states is consistent with the fact that the Horie-Ogawa calculation is not capable of describing them. Those states are also reproduced as well as the k = 0 dominant ones. The present calculation is undoubtedly more successful than any other calculation that has ever been reported in this mass region.

In order to study the E2 properties, we have calculated the effective charges by applying Sagawa and Brown's HF+RPA method. The measured E2 moments and transition rates are reproduced fairly well, by the shell model wavefunctions together with the microscopic effective charges. The M1 properties have also been investigated by using Towner's microscopic parameters. This approach gives an overall agreement with experiment. There remains, however, some discrepancies in the electromagnetic properties. Most of the discrepancies seem to be due to the influence of the k > 2 or the sd-shell configurations. The overall reproduction of the electromagnetic properties has confirmed the reliability of the shell model wavefunctions.

The (e, e') C2 form factors have also been calculated in the same framework as the E2 properties. Together with the (p, p') results, we have confirmed that the quadrupole collective features are successfully described by the present shell model wavefunctions.

We have investigated the low-lying states of the nuclei in the middle of the pf-shell, from a microscopic standpoint. The present effective interaction is derived on a realistic basis, without fitting two-body matrix elements to observed energy levels, although there remains an uncertainty in the G-matrix calculation. By applying this interaction, some of real situations of the low-lying states of the middle pf-shell nuclei are successfully reproduced. It is remarked that the large-scale calculation including the excitation from  $0f_{7/2}$  to  $(0f_{5/2}1p_{3/2}1p_{1/2})$  up to two nucleons is crucial for this agreement. The successful results of this study enable us to place confidence, to a certain extent, in the ways of understanding the nuclear many-body system from the nucleonic degrees of freedom.

The authors are grateful to Prof. H. Sagawa for valuable discussion of the HF+RPA calculation. The authors thank Prof. A. Gelberg for careful reading the manuscript. The computers used for the numerical calculations are HITAC-S820/80 in Computer Center,

University of Tokyo, HITAC-S820/80 in Kanagawa Factory, Hitachi Corporation, and VAX6440 in Meson Science Laboratory, University of Tokyo. This work is financially supported, in part, by Research Center for Nuclear Physics, Osaka University.

## References

- [1] B. A. Brown and B. H. Wildenthal, Ann. Rev. Nucl. Part. Sci. **38**(1988)29
- [2] T. T. S. Kuo and G. E. Brown, Nucl. Phys. 85(1966)40;
   T. T. S. Kuo, Nucl. Phys. A103(1967)71
- [3] J. D. McCullen, B. F. Bayman and L. Zamick, Phys. Rev. 134(1964)B515;
   J. N. Ginocchio, Phys. Rev. 144(1966)952
- [4] J. Vervier, Nucl. Phys. **78**(1966)497
- [5] S. Cohen *et al.*, Phys. Rev. **160**(1967)903;N. Auerbach, Phys. Rev. **163**(1967)1203
- [6] H. Horie and K. Ogawa, Prog. Theor. Phys. 46(1971)439
- [7] H. Horie and K. Ogawa, Nucl. Phys. A216(1973)407;
   N. Bendjaballah et al., Nucl. Phys. A284(1977)513
- [8] H. Nakada, T. Otsuka and T. Sebe, Phys. Rev. Lett. 67(1991)1086;
  H. Nakada, Ph. D. thesis (University of Tokyo, 1991);
  H. Nakada, T. Otsuka and T. Sebe, in AIP conference proceedings 238: Capture Gamma-Ray Spectroscopy, ed. by R. W. Hoff (American Institute of Physics, 1991), p.131
- [9] S. A. A. Eid, W. D. Hamilton and J. P. Elliott, Phys. Lett. **B166**(1986)267
- [10] S. P. Collins et al., J. Phys. **G15**(1989)321
- [11] K. P. Lieb et al., Phys. Lett. **B215**(1988)50

- [12] J. Takamatsu et al., Colloque de Physique C6(1990)423;
   J. Takamatsu, Ph. D. thesis (Tohoku University, 1991)
- [13] T. T. S. Kuo and G. E. Brown, Nucl. Phys. **A114**(1968)241
- [14] T. Motoba and K. Itonaga, Suppl. Prog. Theor. Phys. 65(1979)136
- [15] E. Pasquini and A. Zuker, in *Physics of Medium-Light Nuclei*, ed. by P. Blasi and R.
   A. Ricci (Editrice Compositori, 1978), p.62
- [16] A. Poves and A. Zuker, Phys. Rep. **70**(1981)235
- [17] J. B. McGrory, B. H. Wildenthal and E. C. Halbert, Phys. Rev. C2(1970)186;
   J. B. McGrory, Phys. Rev. C8(1973)693
- [18] G. Oberlechner and J. Richert, Nucl. Phys. A191(1972)577
- [19] B. J. Raz and M. Soga, Phys. Rev. Lett. 15(1965)924;
  - T. Engeland and E. Osnes, Phys. Lett. **20**(1966)424;
  - N. Auerbach, Phys. Lett. **B24**(1967)260;
  - K. Lips and M. T. McEllistrem, Phys. Rev. C1(1970)1009;
  - T. Oda, K. Muto and H. Horie, Lett. Nuovo Cimento 18(1977)549;
  - A. Yokoyama, T. Oda and H. Horie, Prog. Theor. Phys. 60(1978)427
- [20] T. Motoba and K. Ogawa, Prog. Theor. Phys. **51**(1974)173;
  - T. Motoba, Prog. Theor. Phys. **54**(1975)429;
  - H. G. Benson and I. P. Johnstone, Can. J. Phys. **53**(1975)1715;
  - R. B. M. Mooy and P. W. M. Glaudemans, Z. Phys. **A312**(1983)59
- [21] K. Muto and H. Horie, Phys. Lett. **B138**(1984)9
- [22] S. S. M. Wong and W. G. Davies, Phys. Lett. **B28**(1968)77
- [23] T. Sebe and J. Nachamkin, Ann. Phys. 51(1969)100;
   R. R. Whitehead, Nucl. Phys. A182(1972)290

- [24] T. T. S. Kuo and E. Osnes, Folded diagram theory of the effective interaction in atomic nuclei, Lecture Notes in Physics, vol.364 (Springer-Verlag, 1990), and references therein
- [25] J. Shurpin, T. T. S. Kuo and D. Strottman, Nucl. Phys. A408(1983)310
- [26] T. W. Burrows, Nucl. Data Sheets 48(1986)569
- [27] T. W. Burrows, Nucl. Data Sheets **61**(1990)1
- [28] Z. Chunmei, Nucl. Data Sheets **63**(1991)229
- [29] H. Junde *et al.*, Nucl. Data Sheets **58**(1989)677
- [30] H. Junde and H. Dailing, Nucl. Data Sheets 61(1990)47
- [31] W. Gongqing, Z. Jiabi and Z. Jingen, Nucl. Data Sheets 50(1987)255
- [32] Z. Enchen et al., Nucl. Data Sheets 44(1985)463
- [33] H. Junde *et al.*, Nucl. Data Sheets **51**(1987)1
- [34] T. W. Burrows and M. R. Bhat, Nucl. Data Sheets 47(1986)1
- [35] L. K. Peker, Nucl. Data Sheets **61**(1990)189
- [36] A. Huck et al., Phys. Rev. C22(1980)2544
- [37] W. A. Richter, M. G. van der Merwe, R. E. Julies and B. A. Brown, Nucl. Phys. A523(1991)325
- [38] T. T. S. Kuo, private communication
- [39] H. Sagawa and B. A. Brown, Nucl. Phys. **A430**(1984)84
- [40] N. van Giai and H. Sagawa, Nucl. Phys. A371(1981)1;
   N. van Giai and H. Sagawa, Phys. Lett. B106(1981)379

- [41] G. F. Bertsch and F. S. Tsai, Phys. Rep. **18**(1975)125
- [42] K. Shimizu and A. Arima, Nucl. Phys. **A227**(1974)357
- [43] L. Niesen and W. J. Huiskamp, Physica 57(1972)1;
  Table of Isotopes, seventh edition, ed. by C. M. Lederer and V. S. Shirley (John Wiley & Sons, 1978)
- [44] I. S. Towner, Phys. Rep. **155**(1987)263
- [45] A. Arima, K. Shimizu, W. Bentz and H. Hyuga, in Advances in Nuclear Physics, ed. by J. W. Negele and E. Vogt, vol.18 (Plenum, 1988), p.1
- [46] K. H. Speidel, et al., Z. Phys. **A342**(1992)17
- [47] S. S. Rosenblum and W. A. Steyert, Phys. Lett. **B55**(1975)450
- [48] A. Richter, in *Proc. of 4th International Spring Seminar on Nuclear Physics: The Building Blocks of Nuclear Structure*, ed. by A. Covello (World Scientific, 1993), p.335
- [49] L. H. Chan et al., Phys. Rev. 141(1966)1298;
   A. Bohr and B. R. Mottelson, Nuclear Structure, vol.1 (Benjamin, 1969), p.386
- [50] L. J. Tassie and F. C. Barker, Phys. Rev. **111**(1958)940
- [51] R. J. Peterson, H. Theissen and W. J. Alston, Nucl. Phys. A153(1970)610;
  J. Heisenberg, J. S. McCarthy and I. Sick, Nucl. Phys. A164(1971)353;
  G. Hartung et al., Phys. Lett. B221(1989)109
- [52] J. W. Lightbody Jr. et al., Phys. Rev. C27(1983)113
- [53] T. de Forest Jr. and J. D. Walecka, Adv. Phys. **15**(1966)1
- [54] Phan-Xuan-Ho, J. Bellicard and Ph. Leconte, Nucl. Phys. A210(1973)189
- [55] J. Heisenberg, in Advances in Nuclear Physics, ed. by J. W. Negele and E. Vogt, vol.12 (Plenum, 1981), p.61

- [56] K. Nakayama and W. G. Love, Phys. Rev. C38(1988)51
- [57] G. Bertsch, J. Borysowicz, H. McManus and W. G. Love, Nucl. Phys. A284(1977)399
- [58] H. V. von Geramb, in The Interaction between Medium Energy Nucleons in Nuclei,
  ed. by H. O. Meyer (American Institute of Physics, 1983), p.44;
  L. Rikus, N. Nakano and H. V. von Geramb, Nucl. Phys. A414(1984)413